The dc electrical coupling of flow vortices and flow channels in the magnetosphere to the resistive ionosphere

Joseph E. Borovsky and John Bonnell[1]

Space and Atmospheric Sciences Group, Los Alamos National Laboratory, Los Alamos, New Mexico

Abstract. The dc electrical coupling of magnetospheric flow vortices and magneto-spheric flow channels to the ionosphere is numerically calculated. The equations governing the coupling are derived from current continuity plus Ohm's laws taken for the regions of field-aligned current between the ionosphere and magnetosphere and for the Pedersen layer of the ionosphere. For vortices the strength of the coupling (as measured by fractional penetration of the magnetospheric electric fields down to the ionosphere and by the amount of power dissipation) varies, as expected, with the size of the vortex footprint in the ionosphere. However, because of the diode-like nature of the field-aligned currents, the coupling also varies with sign of the vorticity: Positive center vortices (vorticity antiparallel to $\vec{B}$) couple much more strongly than do negative center vortices (vorticity parallel to $\vec{B}$). Negative center vortices tend to dissipate most of their energy in parallel currents, whereas positive center vortices dissipate most of their energy in Pedersen currents. The electric fields of positive center vortices spread across $\vec{B}$ as they connect to the ionosphere, whereas the electric fields of negative center vortices stay confined to their magnetic footprints. Consequently, positive center vortices in the magnetosphere produce quasi-circular vortices of flow in the ionosphere whereas negative center vortices in the magnetosphere produce narrow east-west-elongated vortices of flow in the ionosphere. Negative center vortices in the magnetosphere could produce east-west-aligned bright arc-like features, and positive center vortices could produce east-west-aligned black-arc features imbedded in large circular patches of aurora. Flow channels in the magnetosphere drive field-aligned currents into the ionosphere: The upward field-aligned current on the negative-charged edge of the channel tends to spread across $\vec{B}$, whereas downward current on the positive charge edge tends to stay confined. In the magnetosphere the current spreading results in a back emf that produces a backward flow outside the flow channel on the negative-charged edge.

1. Introduction

With the calculations contained in this paper, one can calculate the amount of power dissipated by a flow vortex in the magnetosphere owing to the electric currents driven in the magnetosphere and ionosphere by the electric field of the vortex. This work is motivated by recent work on the turbulence in the Earth's plasma sheet. Observations of flow velocities and magnetic fields in the near-Earth plasma sheet indicate that the plasma sheet is turbulent in the MHD range of frequencies [*Funsten et al.*, 1995; *Borovsky et al.*, 1997]. It has not been conclusively determined whether the turbulence in the

plasma sheet is composed of Alfven waves or of vortices, although arguments can be made that Alfven waves of the necessary frequency do not fit within the plasma sheet, leaving vortices as the prime candidate. When attempting to analyze this turbulence in the magneto-tail plasma sheet, one big question is how the turbulence (vortices) dissipates. Since the plasma is collisionless, the viscosity calculated from Coulomb collisions is very weak, leading to estimates that the turbulent Reynolds number is enormous [it Borovsky et al., 1997] (see also *Montgomery* [1987]) and that internal dissipative mechanisms are ineffective. A leading candidate for dissipation of the vortices composing the plasma sheet turbulence is nonlocal magnetosphere-ionosphere coupling. This coupling of a vortex to the ionosphere has two aspects: (1) a transmission-line problem to determine the time evolution of the coupling currents [cf. *Goertz and Boswell*, 1979; *Haerendel*, 1983; *Lysak*, 1990] and (2) a mapping problem to determine the steady state current pattern driven in the magnetosphere-ionosphere system and the amount of power dissipation in that current

system. This paper concerns the second aspect. The transmission-line problem, which deals with the propagation of ducted Alfven waves between the magnetosphere and the ionosphere and which deals with Alfven-wave reflectivity off the ionosphere, will be dealt with in a subsequent paper.

There is an established one-dimensional (in the ionosphere) picture of static magnetosphere-ionosphere coupling [e.g. *Lyons*, 1980, 1981; *Chiu and Cornwall*, 1980; *Newman et al.*, 1986]. (See also *Zhang and Cole* [1987] for an analogous picture of upper-to-lower ionosphere coupling.) That picture predicts that magnetospheric features (flows or perpendicular electric fields) that have large magnetic footprints in the ionosphere map well to the ionosphere, whereas magnetospheric features that have small magnetic footprints are largely disconnected from the ionosphere by parallel potential drops (see also *Goertz* [1985] and *Weimer et al.* [1985]. When attempting to estimate the power dissipation driven by the dc currents connecting a magnetospheric vortex to the ionosphere, the well-established one-dimensional (in the ionosphere) pictures of static magnetosphere-ionosphere coupling [e.g. *Lyons*, 1980,1981; *Chiu and Cornwall*, 1980; *Newman et al.*, 1986] were problematic in that a vortex in the magnetosphere maps to an east-west-aligned elongated structure in the ionosphere and one does not know, offhand, whether to use the east-west or the north-south ionospheric scale size for the mapping. (The north-south electric field is concentrated by the mapping but it penetrates down poorly, and the east-west electric field is weakened by the mapping but penetrates down well.) As will be seen in this paper, the vortex-mapping picture is complicated well beyond the mere question of which scale size to use: Vortices with positive-charge centers (vorticity antiparallel to $\vec{B}$) and vortices with negative-charge centers (vorticity parallel to $\vec{B}$) couple very differently to the ionosphere (see Table 1).

In this paper, the one-dimensional (i.e., north-south) theoretical picture of the static coupling of magnetospheric electric fields to the ionosphere [*Lyons*, 1980, 1981; *Chiu and Cornwall*, 1980; *Goertz*, 1985] is generalized to two dimensions (north-south and east-west). The one-dimensional picture, a simple circuit (see Figure 1), is developed by algebraically combining an Ohm's law for upward field-aligned currents (a Knight relation [*Knight*, 1973]), an Ohm's law in the ionosphere for Ped-

ersen currents, a current-continuity relation, and Kirchoff's voltage law $\oint \vec{E} \cdot d\vec{\ell} = 0$. (A brief derivation of the magnetosphere-ionosphere coupling with this circuit can be found in section 3.1 of *Borovsky* [1993].) The two-dimensional picture in this paper is constructed similarly by assuming that currents flow ohmically in the ionosphere and ohmically along the magnetic field lines between the magnetosphere and ionosphere. Current continuity is invoked everywhere, and by assuming that all electric fields are electrostatic an elliptic partial differential equation is developed for the electrostatic potential in two dimensions in the ionosphere with a source term that is the electrostatic potential in the magnetosphere in two spatial dimensions transverse to $\vec{B}$. The elliptic equation is numerically solved.

The reader is reminded that the picture explored here will be static, ignoring the complications of turn-on effects, circuit ringing, Alfven-wave reflectance, etc. [cf. *Goertz and Boswell*, 1979; *Haerendel*, 1983; *Lysak*, 1990].

This paper is organized as follows. In section 2.1 the two-dimensional static coupling equations are derived and the method of computational solution is discussed, and in section 2.2 the calculation of the power dissipation in the magnetosphere-ionosphere currents is discussed. In section 3 the coupling of magnetospheric flow vortices to the ionosphere is examined: Section 3.1 deals with the idealized case of vortices that have magnetic footprints that are circular in the ionosphere, and section 3.2 deals with the more-realistic case of vortices with elongated ionospheric footprints. In section 4 the coupling of magnetospheric flow channels to the ionosphere is examined. In section 5 the gross effects of relaxing the condition that the downward field-aligned current regions are infinitely conducting are examined. Two example vortices (one positive centered and one negative centered) with realistic parameters in the magnetosphere and the ionosphere are examined in detail in section 6. In section 7 the results are summarized and some predictions for observations are made. Table 1 compares some of the gross properties of positive center and negative center vortices, and Table 2 collects the detailed parameters of an example positive center vortex and an example negative center vortex.

2. Derivations and Computation

The problem to be treated is one in which the electrostatic potential (and so the perpendicular electric field)

Table 1. Vortex Types

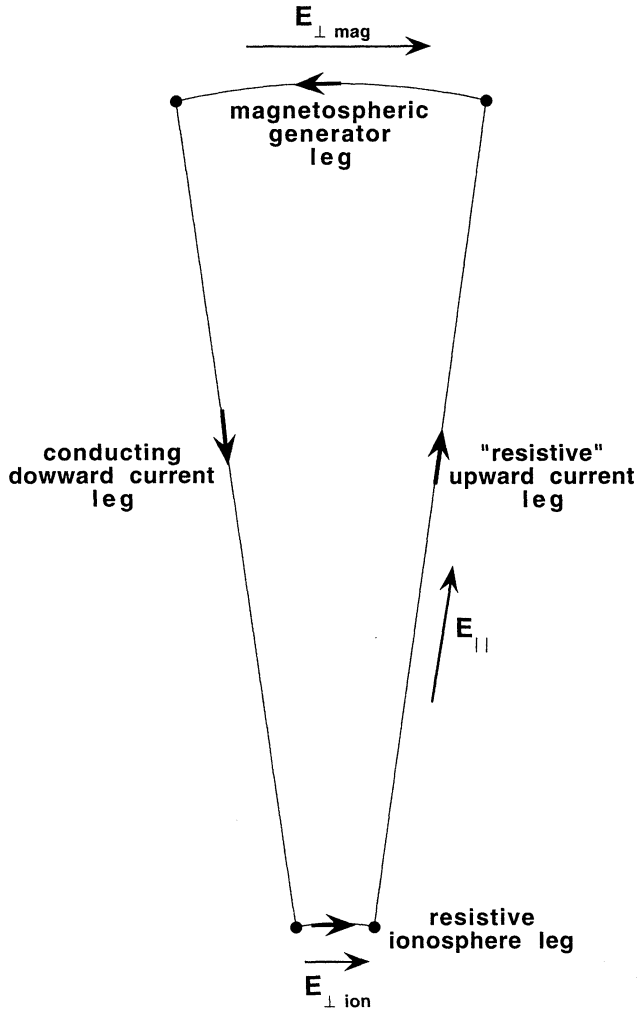| Vortex Type	$\vec{\Omega} : \vec{B}$ in the Vortex	Connection to the Ionosphere	Currents Driven	Damping of Vortex	Spreading Across $\vec{B}$
positive center	antiparallel	good	large	strong	yes
negative center	parallel	poor	weak	weak	no

Figure 1. A sketch of a one-dimensional (in the ionosphere) current system driven by an electric field in the magnetosphere perpendicular to $\vec{B}$.

is given everywhere in the magnetosphere. The magnetospheric potential is associated with $\vec{E} \times \vec{B}$ drift flow in the magnetosphere. This potential pattern in the magnetosphere is magnetically connected to the ionosphere, and so the magnetospheric electric fields drive currents: upward and downward field-aligned currents between the magnetosphere and the ionosphere and Pedersen currents within the ionosphere, as in Figure 1, but now generated for potentials that vary in both directions perpendicular to $\vec{B}$. It will turn out that the derivation is insensitive as to whether the magnetic field lines are straight or curved,; the critical aspect is the size (and shape) of the magnetic footprint of the vortex in the ionosphere. In section 2.1 the equation that will yield the electrostatic potential pattern in the ionosphere caused by an electrostatic potential pattern applied in the magnetosphere is derived, and the method of computational solution of the equation is described. In section 2.2 the method for determining the power dissipation rate of a vortex of $\vec{E} \times \vec{B}$ drift flow in the magnetosphere is described.

2.1. Derivation of the Coupling Equations

Ignoring Hall effects, the horizontal current density $\vec{j}_\perp(x, y)$ in the ionosphere is given by

$$\vec{j}_\perp = \sigma_P \, \vec{E}_{\perp \mathrm{ion}}, \qquad (1)$$

where σ_P is the Pedersen conductivity and $\vec{E}_{\perp \mathrm{ion}}(x, y)$ is the horizontal electric field in the ionosphere that is driven by the magnetospheric electric field. The horizontal coordinates (x, y) are taken to be in the ionosphere. In the upward current regions, the field-aligned current density out of the topside of the ionosphere is given by a Knight relation [e.g., *Antonova and Tverskoy*, 1975; *Lyons*, 1980; *Chiu and Cornwall*, 1980; *Dors and Kletzing*, 1999]:

$$j_\parallel = Q_{\mathrm{up}} \left[\phi_{\mathrm{ion}}(x, y) - \phi_{\mathrm{mag}}(x, y) \right], \qquad (2)$$

where $\phi_{\mathrm{ion}}(x, y)$ is the electrostatic potential in the ionosphere at point (x, y), where $\phi_{\mathrm{mag}}(x, y)$ is the electrostatic potential in the magnetosphere on the field line that maps to (x, y) in the ionosphere, and where $Q_{\mathrm{up}} \approx n e^2 / m_e v_{\mathrm{Te}}$ [cf. *Borovsky*, 1993], with n and v_{Te} being the electron density and electron thermal velocity $(k_B T_e / m_e)^{1/2}$ in the magnetosphere. At each point that has an upward current, $\phi_{\mathrm{ion}} > \phi_{\mathrm{mag}}$. In the downward current or zero-current regions, where the field-aligned conductivity is $Q_{\mathrm{down}} \sim \infty$,

$$\phi_{\mathrm{ion}}(x, y) = \phi_{\mathrm{mag}}(x, y). \qquad (3)$$

In the ionosphere the current-continuity relation $\nabla \cdot \vec{j} = 0$ is

$$\frac{\partial j_x}{\partial x} + \frac{\partial j_y}{\partial y} + \frac{\partial j_z}{\partial z} = 0. \qquad (4)$$

The Pedersen current densities j_x and j_y are given by expression (1): $j_x = \sigma_P E_{x \, \mathrm{ion}}$ and $j_y = \sigma_P E_{y \, \mathrm{ion}}$. Using these and expression (2) for $j_z = j_\parallel$, expression (4) becomes

$$\frac{\partial}{\partial x} \left[\sigma_P E_{x \, \mathrm{ion}} \right] + \frac{\partial}{\partial y} \left[\sigma_P E_{y \, \mathrm{ion}} \right]$$

$$+ \frac{\partial}{\partial z} \left[Q_{\mathrm{up}} \left(\phi_{\mathrm{ion}} - \phi_{\mathrm{mag}} \right) \right] = 0. \qquad (5)$$

Integrating $\int dz$ from the bottom to the top of the Pedersen layer (where $j_\parallel = 0$ at the bottom of the layer), assuming that $E_{x \, \mathrm{ion}}$ and $E_{y \, \mathrm{ion}}$ are independent of z within the ionosphere, and taking the Pedersen conductivity σ_P to be independent of x and y, expression (5) becomes

$$\Sigma_P \frac{\partial E_{x \, \mathrm{ion}}}{\partial x} + \Sigma_P \frac{\partial E_{y \, \mathrm{ion}}}{\partial y} \pm Q_{\mathrm{up}} \left(\phi_{\mathrm{ion}} - \phi_{\mathrm{mag}} \right)$$

$$= 0, \qquad (6)$$

where Σ_P is the height-integrated Pedersen conductivity [cf. *Bostrom*, 1973]. Taking $\vec{E}_{\perp \, ion} = -\nabla_\perp \phi_{\mathrm{ion}}$, expression (6) can be written

$$\nabla^2_\perp \; \phi_{\mathrm{ion}} \;\; \mp \;\; \frac{Q_{\mathrm{up}}}{\Sigma_\mathrm{P}} \; \phi_{\mathrm{ion}} \;\; \pm \;\; \frac{Q_{\mathrm{up}}}{\Sigma_\mathrm{P}} \; \phi_{\mathrm{mag}} \;\; = \;\; 0, \qquad (7)$$

where $\phi_{\mathrm{ion}} = \phi_{\mathrm{ion}}(x,y)$ is the (unknown) electrostatic potential at the location (x,y) in the ionosphere and $\phi_{\mathrm{mag}} = \phi_{\mathrm{mag}}(x,y)$ is the (known) electrostatic potential in the magnetosphere that is magnetically connected to the location (x,y) in the ionosphere.

Expression (7), an elliptical equation for $\phi_{\mathrm{ion}}(x,y)$ that is driven by $\phi_{\mathrm{mag}}(x,y)$, is computationally solved by converting it into the diffusion (heat) equation [cf. *Roache*, 1976]

$$\frac{\partial \phi_{\mathrm{ion}}(x,y,t)}{\partial t}$$
$$= \; \epsilon \left[\nabla^2_\perp \; \phi_{\mathrm{ion}} \; \mp \; \frac{Q_{\mathrm{up}}}{\Sigma_\mathrm{P}} \; \phi_{\mathrm{ion}} \; \pm \; \frac{Q_{\mathrm{up}}}{\Sigma_\mathrm{P}} \; \phi_{\mathrm{mag}} \right], \quad (8)$$

and letting an initial guess for $\phi_{\mathrm{ion}}(x,y,t=0)$ relax into its $t \to \infty$ asymptotic solution, which is a solution to the elliptic equation, expression (7). In expression (8) the constant ϵ is chosen to ensure slow relaxation (numerical stability). The restriction

$$\phi_{\mathrm{ion}}(x,y) \;\; \geq \;\; \phi_{\mathrm{mag}}(x,y) \qquad (9)$$

is implemented at every time step grid point by grid point by setting $\phi_{\mathrm{ion}}(x,y) = \phi_{\mathrm{mag}}(x,y)$ wherever expression (9) is violated. This is equivalent to implementing expressions (2) and (3) for the upward- and downward current regions.

In expression (8) the height-integrated Pedersen conductivity Σ_P and the field-line conductance Q_{up} combine to form a characteristic scale length in the ionosphere $\ell_\perp$, which can be defined as [e.g., *Lyons*, 1980; *Chiu et al.*, 1981; *Goertz*, 1985]

$$\ell_\perp \;\; = \;\; \left(\frac{\Sigma_\mathrm{P}}{Q_{\mathrm{up}}} \right)^{1/2}. \qquad (10)$$

For the solutions to expressions (8) and (9) in this paper, the height-integrated Pedersen conductivity will be chosen to be $\Sigma_\mathrm{P} = 2.3 \times 10^{12}$ cm/s $= 5$ ohm^{-1} (which is appropriate for a region of the nightside ionosphere that experiences weak auroral precipitation [e.g., *Robinson et al.*, 1981]), and the field-line conductance will be chosen to be $Q_{\mathrm{up}} = 6.8 \times 10^{-2}$ cm^{-1} s^{-1} $= 8 \times 10^{-10}$ mho/m^2, which is appropriate to a magnetospheric plasma with an electron temperature $T_e = 700$ eV and a density $n = 0.3$ cm^{-3} [e.g., *Borovsky et al.*, 1998]. These combine to produce a characteristic scale size $\ell_\perp = 79$ km in the ionosphere.

Some one-dimensional (i.e., $\partial/\partial y = 0$) solutions to equation (7) can be seen in the literature; see, for example Figure 4 of *Lyons* [1980] and Figure 2 of *Chiu et al.* [1981] (without the implementation of expression (9)).

Solutions to expressions (8) and (9) for vortices in the magnetosphere and flow channels in the magnetosphere are discussed in sections 3 and 4, respectively.

2.2. Calculating the Ohmic Power Dissipation of a Vortex

A vortex in the magnetosphere acts as an electrical generator and drives field-aligned currents that close in the ionosphere. Driving these currents through the resistive ionosphere requires power, which comes at the expense of the kinetic energy of the magnetospheric vortex.

When calculating the amount of power P dissipated from a vortex, it is convenient to separately calculate the power dissipation in the ionospheric currents P_{ion} and the power dissipation in the field-aligned currents $P_\|$, where

$$P \;\; = \;\; P_{\mathrm{ion}} \;\; + \;\; P_\|. \qquad (11)$$

The amount of power dissipated in the ionosphere is calculated by integrating $\vec{j} \cdot \vec{E}$ over all of the currents driven in the ionosphere by the vortex, that is,

$$P_{\mathrm{ion}} \;\; = \;\; \int\!\!\int\!\!\int \vec{j}_{\mathrm{ion}} \cdot \vec{E}_{\mathrm{ion}} \; dx \, dy \, dz. \qquad (12)$$

Taking the vertical (z direction) electric field to be small in the ionosphere so that $j_{\|\mathrm{ion}} E j_{\|\mathrm{ion}}$ is negligible, using expression (1) to write $\vec{j}_{\perp_{ion}} = \sigma_\mathrm{P} \vec{E}_{\perp_{ion}}$ in the ionosphere, and taking $\vec{E}_{\perp\mathrm{ion}}$ to be independent of z in the ionosphere, expression (12) becomes

$$P_{\mathrm{ion}} \;\; = \;\; \Sigma_\mathrm{P} \int\!\!\int E^2_{\perp_{ion}} \; dx \, dy, \qquad (13)$$

where Σ_P is the height-integrated Pedersen conductivity of the ionosphere. Again, Σ_P has been taken to be independent of x and y.

The amount of power dissipated in the field-aligned currents driven by the vortex is given by

$$P_\| \;\; = \;\; \int\!\!\int j_\| \, \Delta\phi_\| \; dx \, dy, \qquad (14)$$

where $\Delta\phi_\|(x,y) = (\phi_{\mathrm{ion}}(x,y) - \phi_{\mathrm{mag}}(x,y))$, and where the coordinates x and y are in the ionosphere. Using expression (2) to write $j_\| = Q_{\mathrm{up}} \Delta\phi_\|$, expression (14) becomes

$$P_\| \;\; = \;\; Q_{\mathrm{up}} \int\!\!\int (\phi_{\mathrm{ion}} - \phi_{\mathrm{mag}})^2 \; dx \, dy. \qquad (15)$$

Again, the field-line conductance Q_{up} has been taken to be independent of x and y.

3. Vortices Connected to the Ionosphere

Owing to the convergence and curvature of magnetic field lines of the magnetosphere, a circular vortex in the magnetosphere will magnetically connect to an east-west aligned oval in the ionosphere (cf. section 7). This oval will be referred to as the magnetic footprint of the vortex. The degree of penetration of the electric field of the magnetospheric vortex into the ionosphere will

be governed by the north-south and east-west sizes of the ionospheric footprint. The fraction of penetration depends on the size of the vortex in the magnetosphere only insofar as it determines the size in the ionosphere, as was the case for the magnetospheric structures of simpler geometry mapping to the ionosphere [e.g., *Goertz*, 1985]. For simplicity, vortices with circular footprints will be examined first, followed by vortices with oval footprints.

3.1. Vortices With Circular Footprints in the Ionosphere

The details of the mapping of electric fields from a magnetospheric vortex to the ionosphere depend strongly on the polarity of the vortex. The polarity will be described as positive centered or negative centered (see Table 1). Sketched in Figure 2, this nomenclature comes about as follows. A flow vortex in the magnetosphere must have a radial electric field so that the plasma of the vortex moves with an $\vec{E} \times \vec{B}$ drift motion across the direction of the local magnetic field $\vec{B}$ within the vortex. This electrostatic field is associated with space charge. For a vortex with angular velocity $\vec{\Omega} = \vec{r} \times \vec{v}$ that is parallel to $\vec{B}$ in the vortex, the center of the vortex will be negatively charged and the outer edge of the vortex will be positively charged, as depicted in the right-hand panel of Figure 2. Conversely, for a vortex that has an angular velocity $\vec{\Omega}$ that is antiparallel to $\vec{B}$ inside the vortex, the center of the vortex will be positively charged and the outer edge of the vortex will be negatively charged, as sketched in the left-hand panel of Figure 2. To prevent confusion, the symbol $\vec{\Omega}$ is used for the angular velocity instead of the more usual $\vec{\omega}$; the symbol $\vec{\omega}$ will be reserved for vorticity $\vec{w} = \nabla \times \vec{v}$ [cf. *Tennekes and Lumley*, 1972; *Tritton*, 1977; *Borovsky and Hansen*, 1998].
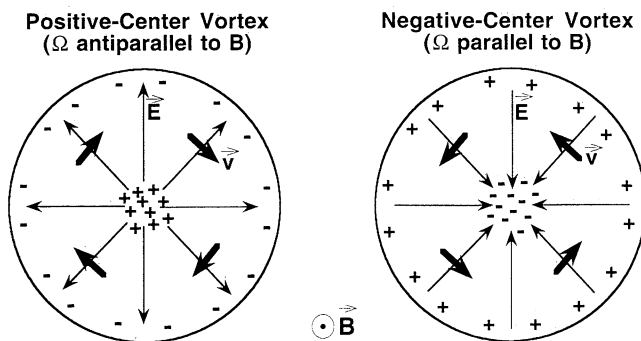
Figure 2. Sketches of (left) a positive center and (right) a negative center vortex in the magnetosphere. The bold short vectors indicate the direction of flow $\vec{V}$ within the vortices, the thin long arrows indicate the direction of the radial electric field $\vec{E}$ within the vortices, and the plus and minus signs indicate the positive and negative charge regions in the vortices. The magnetic field $\vec{B}$ is out of the page as indicated. The picture is consistent in that $\vec{v}$ is given by $\vec{E} \times \vec{B}$ and $\vec{E}$ arises from the charge.
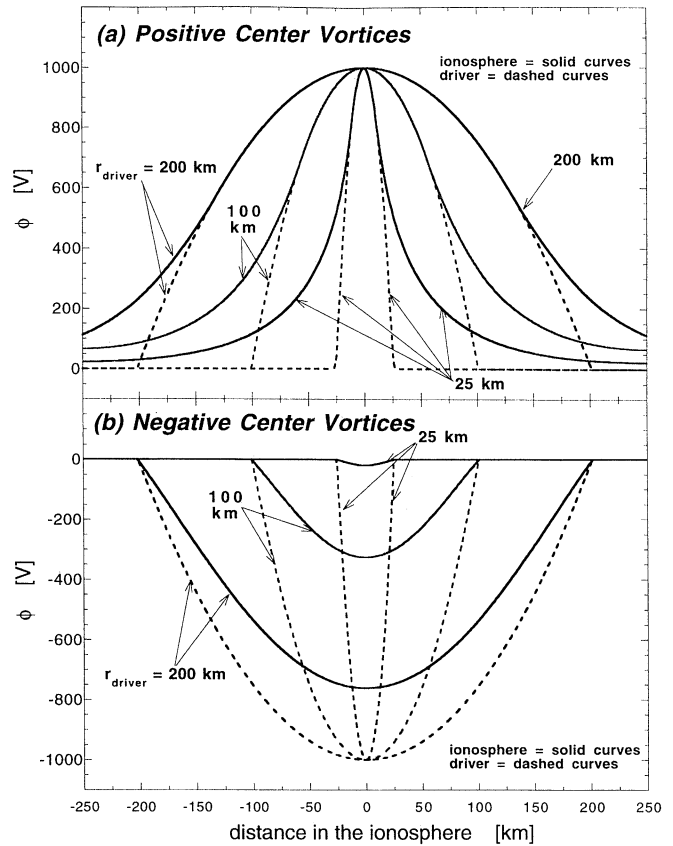
Figure 3. For (a) three positive center vortices and (b) three negative center vortices, the electrostatic potential ϕ of the driver (dashed curves) and the electrostatic potential ϕ in the ionosphere (solid curves) are plotted as functions of the distance in the ionosphere. The vortices are idealized to have circular magnetic footprints in the ionosphere, and the radii of those footprints are 25 km, 100 km, and 200 km in the ionosphere.

In Figures 3a and 3b, positive center and negative center vortices, respectively, are examined. These vortices all have circular footprints. The negative center vortices will be examined first. In Figure 3b the potentials for three different negative center vortices are plotted as functions of the distance x in the ionosphere for a cut through the center of the vortices. The dashed curves are the potentials in the magnetosphere (driver potential) and the solid curves are the potentials in the ionosphere (mapped potential). In all three cases the potential of the vortex center in the magnetosphere is -1000 V and the potential of the vortex edge in the magnetosphere is 0 V. The potential profile in the vortex is chosen to correspond to a solid-body $\vec{E} \times \vec{B}$ rotation out to the vortex edge, where the rotation abruptly drops off to zero. Notice that the condition $\phi_{ion}(x, y) \geq \phi_{mag}(x, y)$ is met. The reader is asked to note two things. First, the potential difference across the vortex in the ionosphere is less than the potential difference in the magnetosphere; that is, the potential difference in the magnetosphere does not entirely map down into the ionosphere. Second, the potential pattern does not

spread across the magnetic field as it maps down to the ionosphere; that is, the potential perturbation in the ionosphere is confined to the magnetic footprint. The fact that the potential difference does not fully map down to the ionosphere means that the electric field $E_{\perp \text{ion}}$ in the ionosphere is weaker than it would have been if there was complete mapping of the magnetospheric potential down to the ionosphere. The $\vec{E} \times \vec{B}$ drift flow pattern in the ionosphere is a vortex flow confined to the magnetic footprint of the magnetospheric vortex, but with an angular velocity that is reduced from that of the magnetospheric vortex owing to the incomplete mapping of the vortex electric field. This means that there is a "slip" of the motion of the magnetosphere relative to the ionosphere, and this slipping is accompanied by a parallel electric field. As can be seen in Figure 3b, the penetration of the potential to the ionosphere is poorer for smaller-sized vortices; that is, there is more slippage for smaller vortices. This reduction in the penetration for smaller vortices will be explored further in this section.

In Figure 3a the potentials for two different positive center vortices are plotted as functions of the east-west distance in the ionosphere: The dashed curves are the potentials in the magnetosphere (driver potentials), and the solid curves are in the ionosphere (mapped potentials). In all of the cases the potential at the center of the vortex in the magnetosphere is +1000 V, and the potential of the outer edge of the vortex in the magnetosphere is 0 V. Again, $\phi_{\text{ion}}(x, y) \geq \phi_{\text{mag}}(x, y)$. The reader is asked to note two things. First, all of the 1000 V of potential drop in the magnetosphere maps to the ionosphere, which is contrary to the case of negative center vortices. Second, the potential pattern of the magnetospheric vortex spreads greatly across the magnetic field as it maps down to the ionosphere, which is also contrary to the case of negative center vortices. The potential pattern in the ionosphere is much larger than the footprint of the vortex itself in the ionosphere. (In the region outside the footprint of the vortex, the ionospheric potential ϕ_{ion} falls off as $r^{-1/2} \exp(-r/\ell_\perp)$, where $\ell_\perp = (\Sigma_\text{P}/Q_{\text{up}})^{1/2}$ is defined in expression (10).) Owing to this spreading of the potential pattern, the electric field $E_{\perp_{ion}}$ in the ionosphere is weaker than it would be if the mapping of the potential did not involve spreading. The weakening of the electric field means that the angular velocity of $\vec{E} \times \vec{B}$ drifting in the ionosphere will be less than it is in the vortex in the magnetosphere. As was the case for negative center vortices, this reduction in electric field means that there is a slippage between the magnetospheric motion and the ionospheric motion. Because of the spreading of the potential, the vortical flow in the ionosphere is larger than the footprint of the magnetospheric vortex.

In Figure 4 the fractional penetration of the vortex electric field from the magnetosphere to the ionosphere is examined. For positive center vortices (squares) and
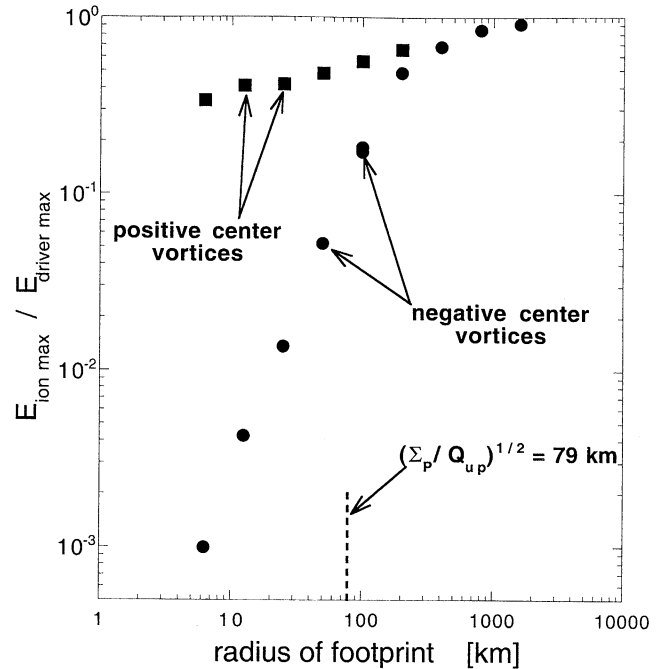

Figure 4. For magnetospheric vortices idealized to have circular magnetic footprints in the ionosphere, the fractional mapping of the electric field down from the magnetosphere is plotted as functions of the radius of the footprint in the ionosphere. The fractional mapping is here denoted as the ratio of the maximum electric field perpendicular to $\vec{B}$ in the ionosphere divided by the maximum of the driver electric field perpendicular to $\vec{B}$. The squares are for positive center vortices and the circles are for negative center vortices.

negative center vortices (circles), the maximum value of the E_{ion} divided by the maximum value of the driver electric field (E_{mag} mapped along the field) is plotted as a function of the radius of the vortex footprint in the ionosphere. If the electric field of the magnetospheric vortex fully penetrated to the ionosphere, the ratio $E_{\text{ion max}}/E_{\text{driver max}}$ would be unity. As can be seen in the figure, for small footprints the electric field penetration to the ionosphere is much poorer for negative center vortices ($\vec{\Omega}$ parallel to $\vec{B}$) than it is for positive center vortices ($\vec{\Omega}$ antiparallel to $\vec{B}$). As can be discerned from the graph, for negative center vortices with small footprints, the electric-field penetration fraction is proportional to the square of the footprint radius in the ionosphere. As also can be discerned from the graph, for positive center vortices, the electric-field penetration fraction is nearly independent of the footprint radius in the ionosphere. This poor connection to the ionosphere for negative center vortices is noted in Table 1.

In Figure 5 the total power dissipation of the ±1000 V vortices are plotted as functions of the radii of the vortex footprints in the ionosphere. Again, the vortices have circular footprints. As can be seen, for small sizes the power dissipation is much greater for positive center vortices ($\vec{\Omega}$ antiparallel to $\vec{B}$) than it is for negative
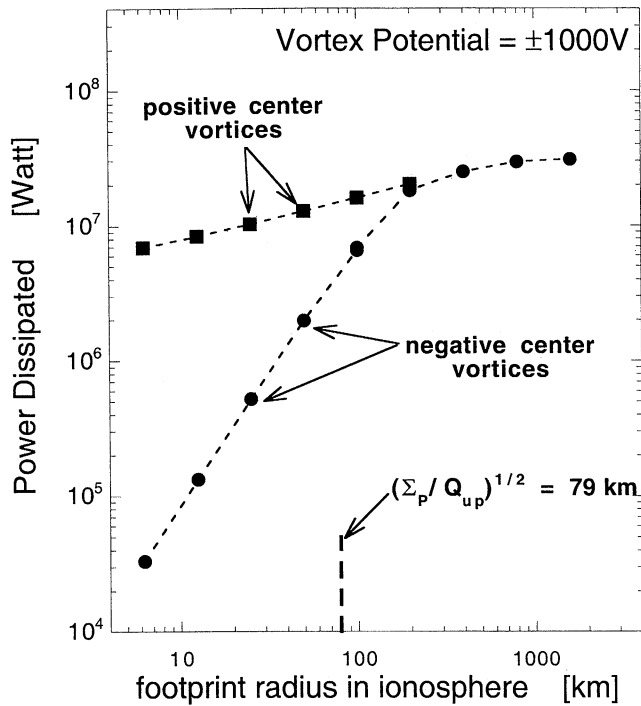
Figure 5. For magnetospheric vortices that are idealized to have circular magnetic footprints in the ionosphere, the total amount of power dissipated P in the current system driven by the vortex is plotted as a function of the radius in the ionosphere of the magnetic footprint of the vortex. The circles are for negative center ($\vec{\Omega}$ parallel to $\vec{B}$) vortices, and the squares are for positive center ($\vec{\Omega}$ antiparallel to $\vec{B}$) vortices. In each case the vortex potential in the magnetosphere is +1000 V or -1000 V.

center vortices ($\vec{\Omega}$ parallel to $\vec{B}$). This is noted in Table 1. For large vortices, or more correctly, for vortices with large magnetic footprints in the ionosphere, the power dissipation is the same for positive center and for negative center vortices. For small vortices the difference in power dissipation is due to the fact that the current system driven by a negative center vortex is weaker than the current system driven by a positive center vortex, so $\int \int \int \vec{j} \cdot \vec{E} \, dx \, dy \, dz$ is weaker. This will be explored further in Figures 6 and 7.

In Figure 6a, for negative center, circular-footprint vortices, the fraction of the total power dissipation that is dissipated in the Pedersen currents of the ionosphere (circles) and the fraction that is dissipated in the upward field-aligned upward currents (triangles) are plotted as functions of the size of the vortex footprint in the ionosphere. As can be seen, for small vortices the dissipation is almost entirely in the field-aligned currents. This indicates that the potential drop of the negative center magnetospheric vortex falls almost entirely in the field-aligned current of the vortex rather than in the Pedersen current. With only weak potential differences driving the Pedersen current, the total current in the "circuit" is small. Hence the total dissipation is small. Note that for large footprint sizes, the ionospheric dis-

sipation dominates (and note from Figure 5 that the total dissipation increases).

In Figure 6b, for positive center, circular-footprint vortices the fractions of the total power dissipation that are dissipated in the Pedersen (circles) and parallel (triangles) currents are plotted as functions of the vortex-footprint radius in the ionosphere. As can be seen, for positive center vortices the power dissipation in the ionosphere dominates the power dissipation in the parallel currents, which is very different from the case of negative center vortices (Figure 6a). Note that the spatial scale of the vortex does not strongly affect the fractional dissipation (at least not for the range of spatial scales explored); this is because, for a small vortex, the potential pattern in the ionosphere is spread to a size much larger than the footprint of the vortex, so the "circuit" behaves, in a sense, like a large-vortex circuit, even when driven by a small vortex. Note that for negative center vortices (Figure 6a) the fraction of power dissipated in parallel currents went to zero as the iono-
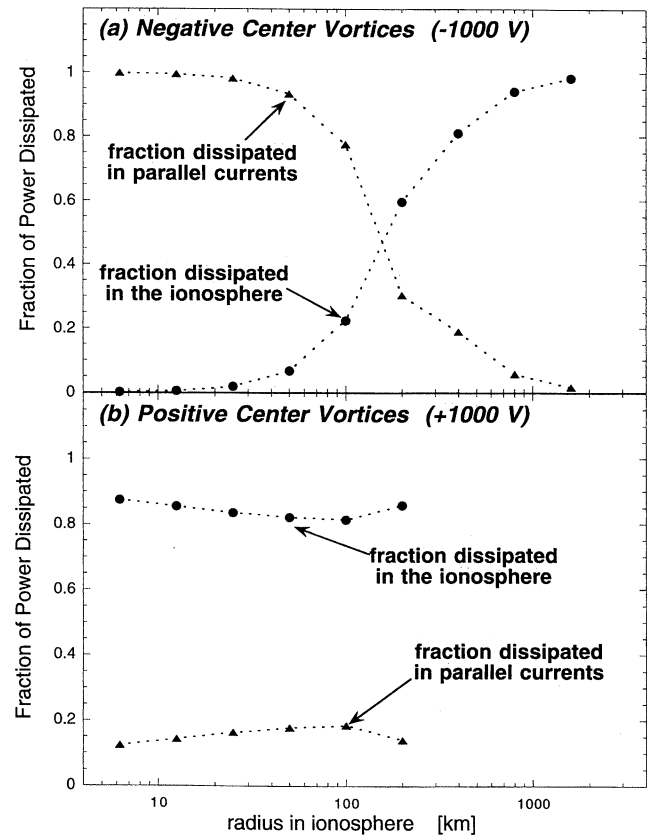

Figure 6. For (a) negative center vortices and (b) positive center vortices the fraction of the total power dissipated that is dissipated in upward field-aligned currents (triangles) and the fraction of the total power dissipated that is dissipated in Pedersen currents (circles) is plotted as a function of the radius of the magnetic footprint in the ionosphere. The negative center vortices all have -1000 V at their centers in the magnetosphere, and the positive center vortices all have +1000 V at their centers in the magnetosphere. The vortices here are idealized to have circular magnetic footprints in the ionosphere.
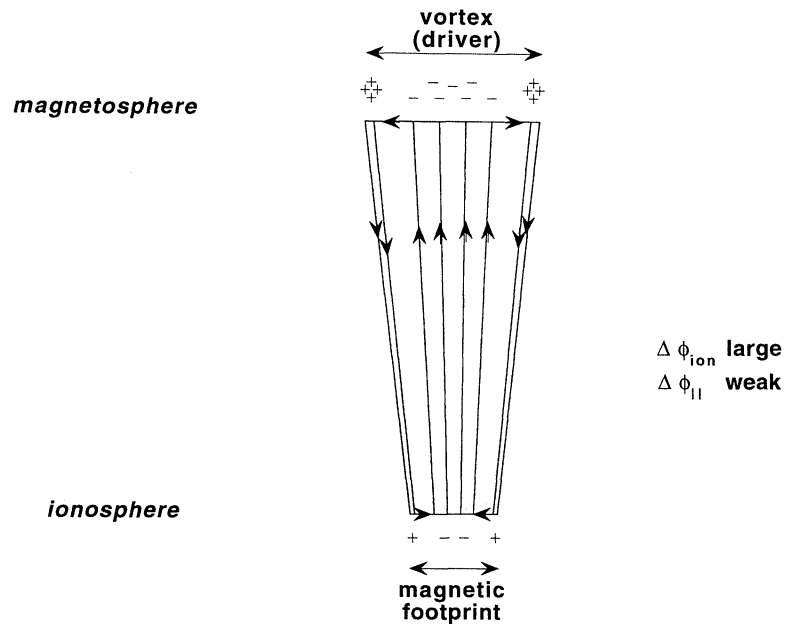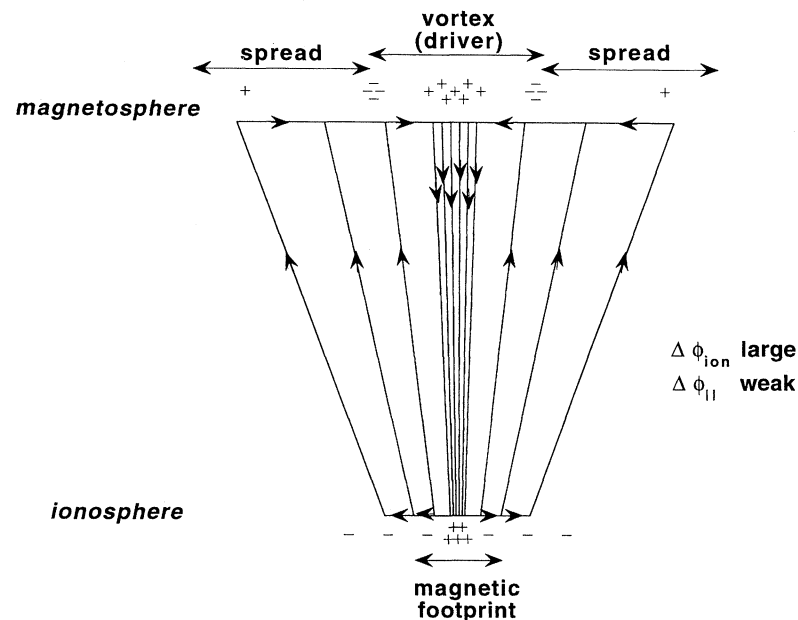
(a) Negative Center Vortex

(b) Positive Center Vortex

Figure 7. A sketch of the current systems driven (a) by a negative center vortex in the magnetosphere and (b) by a positive center vortex in the magnetosphere. The convergence of magnetic field lines from the magnetosphere to the ionosphere is indicated. Note that the current system driven by the negative center vortex is confined along $\vec{B}$ within the magnetic footprint of the vortex (Figure 7a), whereas the current system driven by the positive center vortex spreads across $\vec{B}$ outside of the magnetic footprint.

spheric radius of the vortex went to zero. There is an indication in the last data point in Figure 6b that for positive center vortices the fraction of power dissipated in the parallel currents is decreasing as the ionospheric size of the vortex increases. Unfortunately, it is computationally very expensive to solve expressions (8) and (9) for large positive center vortices since a large grid is required and the relaxation toward a solution is slow on large spatial scales, and so this trend has not been further explored (a brief theoretical treatment of this large-footprint limit appears in section 4 of *Pudovkin et al.* [1997]).

In the two sketches of Figure 7, the current systems ("circuits") that are driven by negative center (Figure 7a) and positive center (Figure 7b) vortices are summarized. The currents are represented by the solid lines in the sketches, the tops of the sketches represent the magnetosphere, and the bottoms represent the ionosphere. The spatial extent of the vortex across $\vec{B}$ is indicated in the top of each sketch. Examining the negative center vortex ($\vec{\Omega}$ parallel to $\vec{B}$) in Figure 7a, it is noted that the center of the vortex has a negative charge and the outer portion has a positive charge. The current system driven by the magnetospheric vortex, which acts to discharge the charge separation of the vortex in the magnetosphere, consists of an upward field-aligned current into the negative-charge region of the vortex center and a downward field-aligned current out of the positively-charged outer region of the vortex. These upward and downward currents close via a Pedersen current across $\vec{B}$ in the ionosphere. In the vortex in the magnetosphere the current closes across $\vec{B}$ as a polarization-drift current in the discharging generator [cf. *Borovsky*, 1987, 1992]. The $\vec{j} \times \vec{B}$ force associated with this polarization-drift current acts to brake the rotational flow of the vortex in the magnetosphere. The electric fields in the current system are not indicated in the sketch, but there is an inward-pointing field $E_{\perp \text{mag}}$ within the vortex in the magnetosphere (which corresponds to the $\vec{E} \times \vec{B}$ rotation of the vortex), there is an upward-pointing field $E_{\parallel}$ in the upward current region, and there is an inward-pointing field $E_{\perp \text{ion}}$ in the ionosphere. The potential drop associated with $E_{\parallel}$ is big, and the potential drop associated with $E_{\perp \text{ion}}$ is small. The total current in the negative-vortex-driven system is weak (because the potential drop in the ionosphere is weak). With time, the charge densities, electric fields, and current densities will all weaken owing to a loss of energy of the vortex that drives the currents. The current in the actual system is almost divergence free, with nonzero divergence associated with the temporal changes in the charge density as the vorticity dissipates owing to a loss of energy. These slow temporal changes are not accounted for in the present treatment.

In Figure 7b the current system driven by a positive center ($\vec{\Omega}$ antiparallel to $\vec{B}$) vortex is sketched. This current system is more complicated than that driven by a negative center vortex. As indicated, the center of the vortex is positively charged and the outer portion is negatively charged. As also indicated, positive charge will begin to buildup in the magnetosphere outside of the original vortex, delivered by field-aligned currents from the ionosphere that are driven by the vortex. A downward field-aligned current connects the positive center of the vortex to the ionosphere. This current connects to a radially outward Pedersen current in the ionosphere, which in turn connects to upward field-aligned currents back into the magnetosphere. Since upward field-aligned current densities are more difficult

to drive than are downward field-aligned current densities (e.g., expression (2)), the region of upward return current tends to be spread in area. These upward currents extend well beyond the magnetic footprint of the vortex, delivering positive space charge into the magnetosphere outside the vortex. The build up of positive charge in this region of the magnetosphere produces an electric field $E_{\perp \text{mag}}$ which corresponds to a rotational flow opposite to the flow of the vortex. Thus as the magnetospheric vortex spins down owing to coupling to the ionosphere, a region of "backspin" will be produced in the magnetosphere outside of the vortex. In the magnetosphere the charge density of the vortex will decrease with time, and charge will build up in the backspin region. The field-aligned currents close across $\vec{B}$ in the magnetosphere in the form of polarization-drift currents. These polarization-drift currents perpendicular to $\vec{B}$ correspond to the $\vec{j} \times \vec{B}$ force that spins down the vortex and the $\vec{j} \times \vec{B}$ force that produces the backspin flow outside the vortex.

In Figure 7b the spreading of the current system and electrostatic potential across the magnetic field $\vec{B}$ is also depicted. This spreading occurs for a positive center vortex but not for a negative center vortex. This fact can be made sense of by considering the diode-like nature of the field-aligned currents: For upward field-aligned currents an Ohm's law holds (expressions (2)), and for downward field-aligned currents infinite conductivity is assumed. The infinite conducting regions of downward field-aligned current act, in a sense, as a shield, enforcing an equipotential between the magnetosphere and the ionosphere. For a negative center vortex the downward field-aligned currents are on the outside of the vortex: thus, all of the electrical perturbation associated with the potential of the magnetospheric vortex is within the shield and so the electrical perturbation does not spread outside of the magnetic footprint. For a positive center vortex, the downward current region is at the center of the vortex: Thus the electrical perturbation of the vortex is outside of the shield, and so the perturbation is unconfined and spreads.

3.2. Vortices With Oval Footprints in the Ionosphere

In Figures 8 and 9 the potential patterns of vortices with oval footprints in the ionosphere are studied. Although more difficult to understand, an oval footprint (from a circular vortex) is more appropriate than a circular footprint for the case of a magnetospheric vortex coupling to the Earth's ionosphere. In Figure 8 a negative center vortex is displayed. Here the east-west-elongated potential is plotted as a function of distance in the ionosphere for cuts in the east-west and north-south directions through the center of the vortex; the dashed curves are the potential in the magnetosphere (driver potential), and the solid curves are the poten-
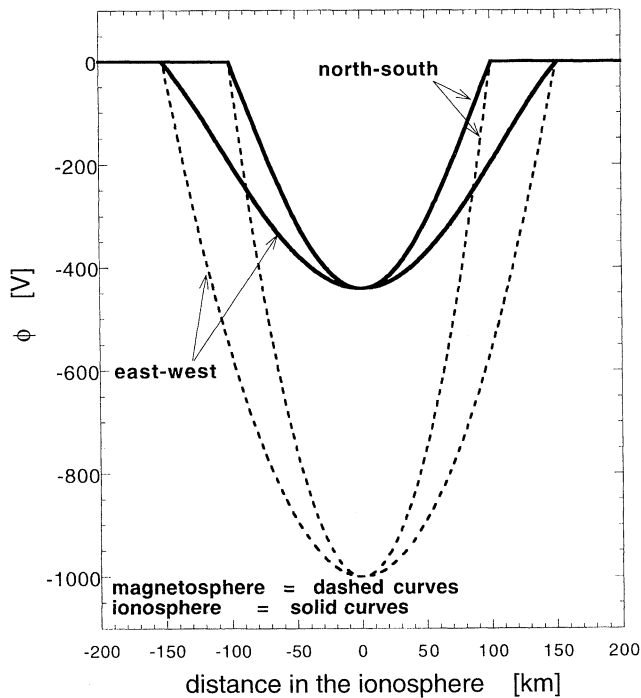
Figure 8. For a negative center magnetospheric vortex that has a magnetic footprint in the ionosphere that is oval shaped, the electrostatic potential ϕ in the ionosphere (solid curves) and the electrostatic potential of the driver (dashed curves) are plotted as functions of the distance in the ionosphere. One set of curves is from a north-south cut through the center of the magnetic footprint, and the other set of curves is from an east-west cut through the center of the magnetic footprint. Note that the full potential of the magnetospheric vortex (-1000 V) does not reach the ionosphere.

tial in the ionosphere, both in ionospheric coordinates. (Note that the vortex is envisioned to be circular in the magnetosphere, but when expressed in ionospheric coordinates the driver is distorted by differing mapping factors in the east-west and north-south directions [e.g., *Kaufmann et al.*, 1990].) In the magnetosphere the center of the vortex is at a potential of -1000 V, and the outer edge of the vortex is at a potential of 0 V. As was the case for the circular-footprint vortices of Figure 3b, the potential difference of the magnetospheric vortex does not fully penetrate to the ionosphere. Note that the potential perturbation in the ionosphere is confined to the magnetic footprint; this means that the $\vec{E} \times \vec{B}$ drift circulation in the ionosphere driven by the vortex will also be confined to the oval footprint.

In Figure 9 the potential of a positive center ($\vec{\Omega}$ antiparallel to $\vec{B}$) vortex with an east-west-elongated footprint is plotted as a function of the distance in the ionosphere for cuts in the east-west and north-south directions through the center of the vortex. The dashed curves are the driver (magnetospheric) potential, and the solid curves are the potentials in the ionosphere. As was the case for the circular-footprint vortices of Figure 3a, the full potential drop of the magnetosphere reaches

the ionosphere but the potential drop spreads across $\vec{B}$ outside of the vortex footprint in the ionosphere. Because the potential perturbation in the ionosphere is not confined to the magnetic footprint, the $\vec{E} \times \vec{B}$ drift circulation in the ionosphere is not confined to the footprint; hence the "vortex" of flow in the ionosphere is larger than the footprint of the magnetospheric vortex.

In Figure 10 the electric fields for negative center (Figure 10a) and positive center (Figure 10b) vortices with oval footprints are examined. In the top plots the driver electric fields (magnetospheric electric field projected along the magnetic field to the ionosphere) are shown and in the bottom plots the electric fields in the ionosphere are shown. Note in the top plots that the strength of the driver electric field increases linearly with distance out from the vortex center: This is the pattern for solid-body rotation under $\vec{E} \times \vec{B}$ drift. In the bottom plot of Figure 10b the ionospheric electric field for the negative center vortex is shown. As can be seen, the strength of the electric field in the ionosphere is much weaker than is the driver field. Near the center of the vortex the electric field increases in strength nearly linearly with distance, which indicates near solid-body rotation for the ionospheric $\vec{E} \times \vec{B}$ flows, but with
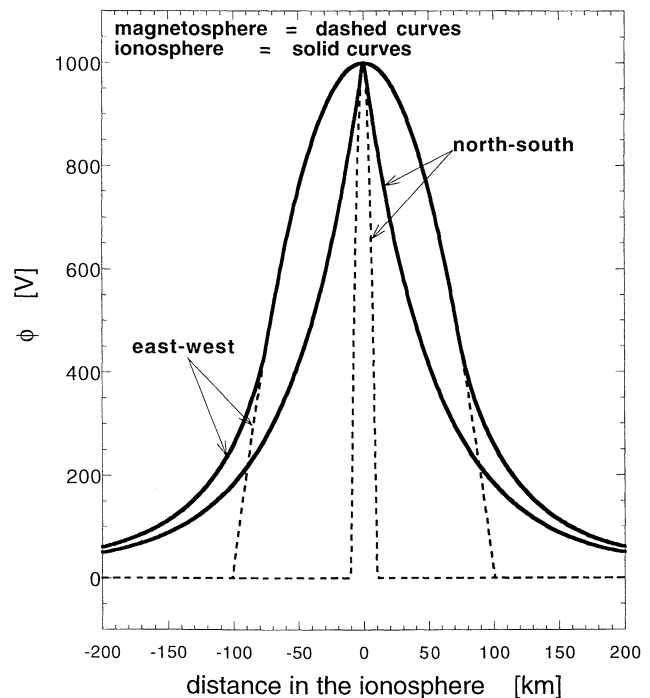

Figure 9. For a positive center magnetospheric vortex that has a magnetic footprint in the ionosphere that is oval shaped, the electrostatic potential ϕ in the ionosphere (solid curves) and the electrostatic potential ϕ of the driver (dashed curves) are plotted as functions of the distance in the ionosphere. One set of curves is from a north-south cut through the center of the magnetic footprint, and the other set of curves is from an east-west cut through the center of the magnetic footprint. Note that the potential pattern of the magnetospheric vortex spreads as it maps down into the ionosphere.
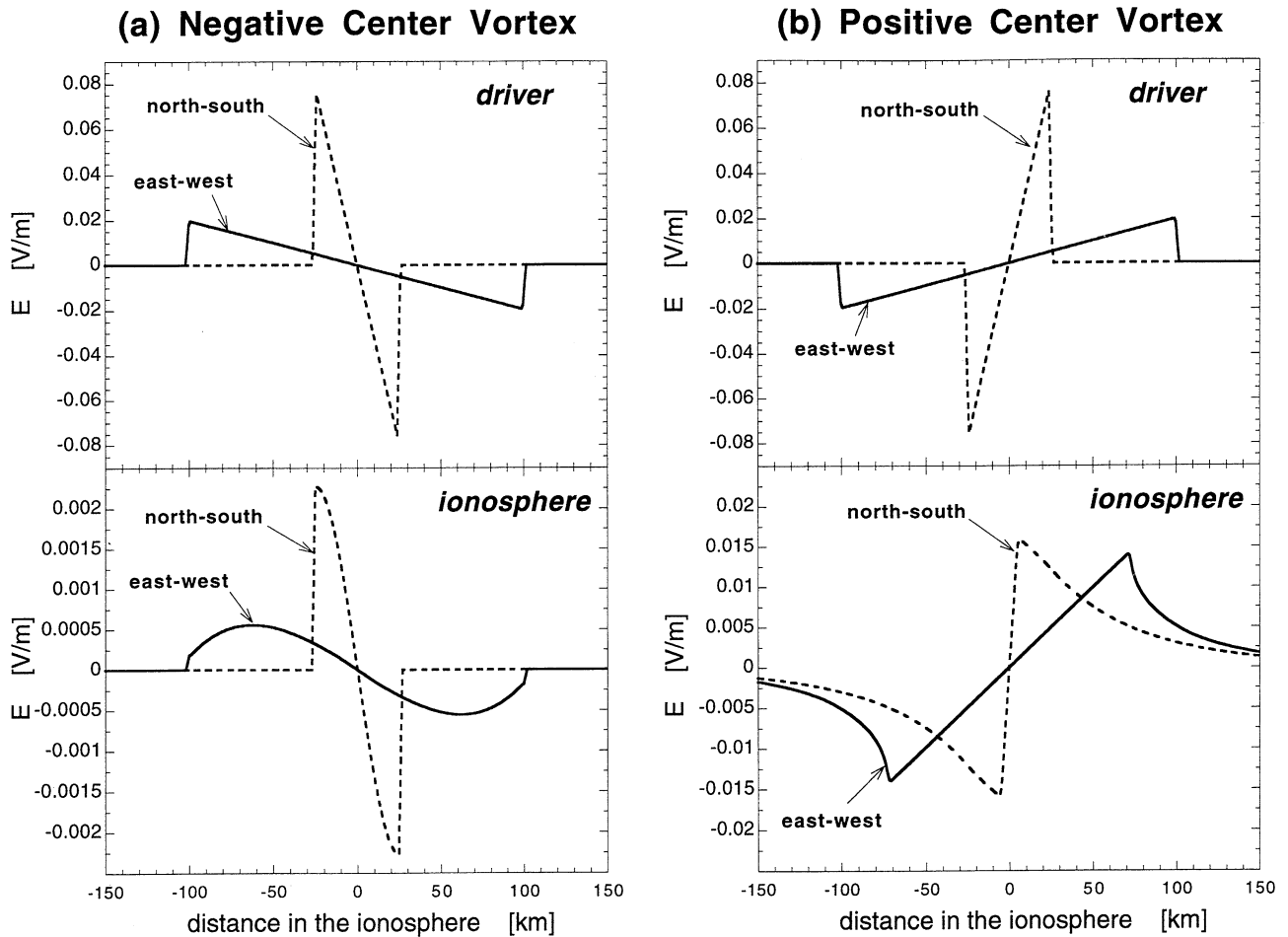
(a) Negative Center Vortex

(b) Positive Center Vortex

Figure 10. For (a) a negative center magnetospheric vortex and (b) a positive center magnetospheric vortex with magnetic footprints in the ionosphere that are ovals, the driver electric fields E (top plots) and the electric fields E in the ionosphere (bottom plots) are shown as functions of the distance in the ionosphere. Each plot is a double plot showning an east-west cut through the center of the magnetic footprint (solid curves) and a north-south cut through the center of the magnetic footprint (dashed curves). Note that the vertical scales differ between the top panels and the bottom panels: The driver electric fields do not fully map down into the ionosphere.

an angular rotation rate Ω that is much slower than the rate in the magnetosphere; that is, there is a lot of slip to the vortical motion when it maps down to the ionosphere. Note, as before, that the electric field in the ionosphere is confined to the magnetic footprint of the vortex for this negative center (Ω parallel to $\vec{B}$) vortex. In the bottom plot of Figure 10b the ionospheric electric field is shown for the positive center vortex. First, note that the electric field extends outside of the magnetic footprint of the vortex. Near the center of the vortex the electric field has the pattern of solid-body rotation, with a sudden deviation from solid-body rotation occurring. As can be discerned from the plot, the region of solid-body rotation is smaller than the magnetic footprint, that is, the breakpoints from solid-body rotation are at radii less than the footprint radii. In the regions of solid-body rotation for the positive center vortex, the angular rotation rate Ω of the $\vec{E} \times \vec{B}$ drift in the ionosphere is the same as the rate in the magnetosphere,

that is, the electric field is fully penetrating in these regions. (Note, however, that the electric field is not very strong in these central regions.) This occurs in a region where $\phi_{\text{ion}}(x, y) = \phi_{\text{mag}}(x, y)$, which is a region near the center of the positive center vortex where the field-aligned current is downward. The regions outside the breakpoints, where the field does not fully map and where solid-body rotation is not occurring, are regions of upward field-aligned currents. Thus in this positive center vortex case the breakpoints in the electric-field pattern divide regions of downward and upward currents.

In Figure 11 the fractional penetration of the electro-static potential (Figure 11a) and the total power dissipation (Figure 11b) are plotted for negative center vortices with oval footprints. Three different series of vortices are plotted: vortices with east-west footprint radii of 100 km in the ionosphere, vortices with east-west radii of 25 km, and vortices with east-west radii
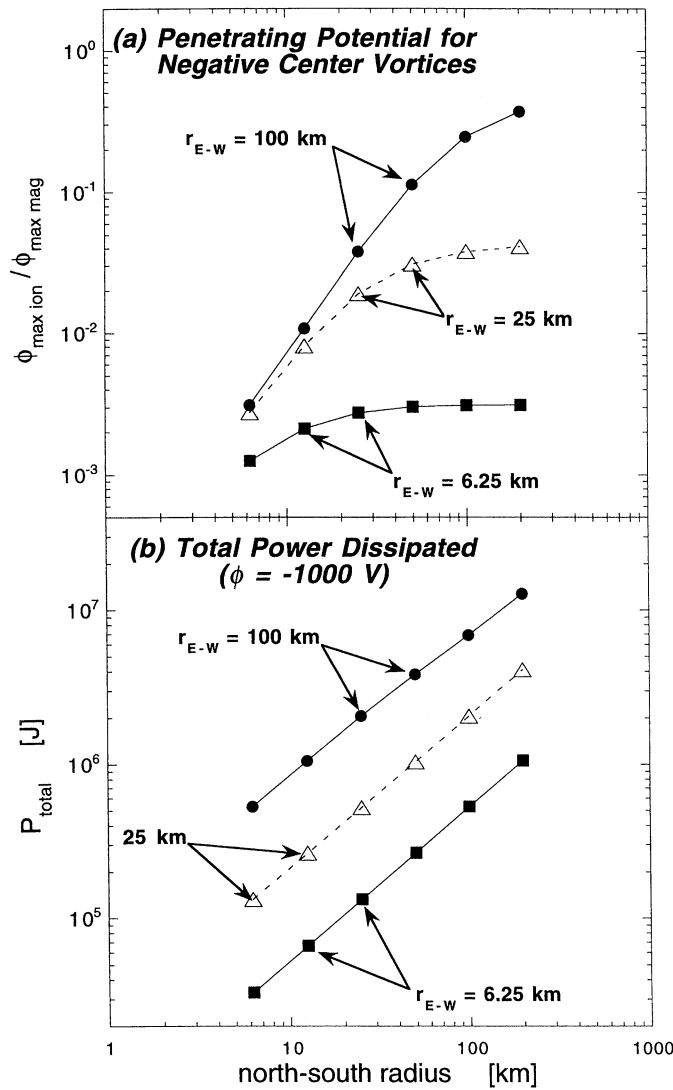
(a) Penetrating Potential for Negative Center Vortices

r_{E-W} = 100 km

r_{E-W} = 25 km

r_{E-W} = 6.25 km

$\phi_{max\ ion}$ / $\phi_{max\ mag}$

(b) Total Power Dissipated (ϕ = -1000 V)

r_{E-W} = 100 km

25 km

r_{E-W} = 6.25 km

P_{total} [J]

north-south radius   [km]

Figure 11. For negative center magnetospheric vortices with oval footprints in the ionosphere, (a) the fractional penetration of the vortex potential down to the ionosphere and (b) the total amount of power dissipated P in the current systems driven by the vortex are plotted as functions of the north-south radius (semiminor or semimajor axis) of the footprint. Three series of curves are run: a series wherein the east-west radius (semimajor or semiminor axis) of the magnetic footprint is 100 km in the ionosphere (circles), a series wherein the east-west radius of the magnetic footprint is 25 km (triangles), and a series wherein the east-west radius of the magnetic footprint is 6.25 km (squares). In each case the potential of the vortex in the magnetosphere is -1000 V.

penetration fraction is only slightly dependent on r_{N-S}. For negative center vortices (and also for positive center vortices), lengthening a footprint does not appreciably increase the penetration of magnetospheric potentials; the fraction of penetration is governed by the narrowest extent of the ionospheric footprint. In Figure 11b the total power dissipated by the negative center magnetospheric vortices is plotted. As can be seen, the larger the footprint of the vortex, the greater the power dissipation. (In this regime of footprint sizes, the total dissipation is dominated by dissipation in the upward field-aligned currents.)

For these same vortices, in Figure 12 the power dissipated is plotted as a function of the area of the magnetic footprint in the ionosphere (squares). Recall that each vortex has a fixed potential of -1000 V at its center. As noted in the figure, for vortices with small footprints, the power dissipated by a negative vortex (of fixed voltage) is directly proportional to area of its footprint.
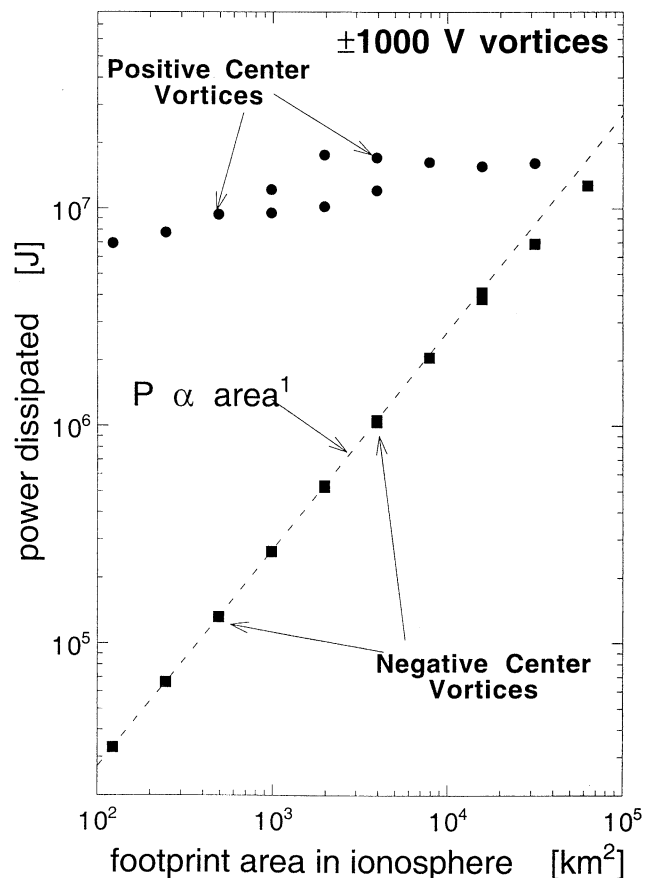

±1000 V vortices

Positive Center Vortices

$P \propto area^1$

Negative Center Vortices

power dissipated [J]

footprint area in ionosphere   [km²]

Figure 12. For a number of positive center magnetospheric vortices (circles) and a number of negative center magnetospheric vortices (squares), the total amount of power dissipated P in the current systems driven by the magnetospheric vortices is plotted as a function of the area in the ionosphere of the magnetic footprint of each vortex. The multiple values of P for a given value of the footprint area come about from vortices with footprints of different shapes but the same areas. A curve with P proportional to area is drawn to guide the eye.

of 6.25 km. In each series the north-south radii of the vortex footprints are varied, and the plots are versus the north-south radius. As can be seen in Figure 11a, the fraction of the magnetospheric-vortex potential that maps down to the ionosphere increases with the north-south radius of the vortex footprint in the ionosphere. In particular, when the north-south radius r_{N-S} is small and smaller than the east-west radius r_{E-W}, the penetration fraction is proportional to r_{N-S}^2. When the north-south radius is greater than the east-west radius, the

(a) Maximum Penetrating Electric Fields for Positive Center Vortices

$E_{ion\ max} / E_{driver\ max}$

$r_{E-W} = 6.25$ km

25 km

$r_{E-W} = 100$ km

(b) Total Power Dissipated ($\phi = +1000$ V)

P_{total} [J]

$r_{E-W} = 100$ km

25 km

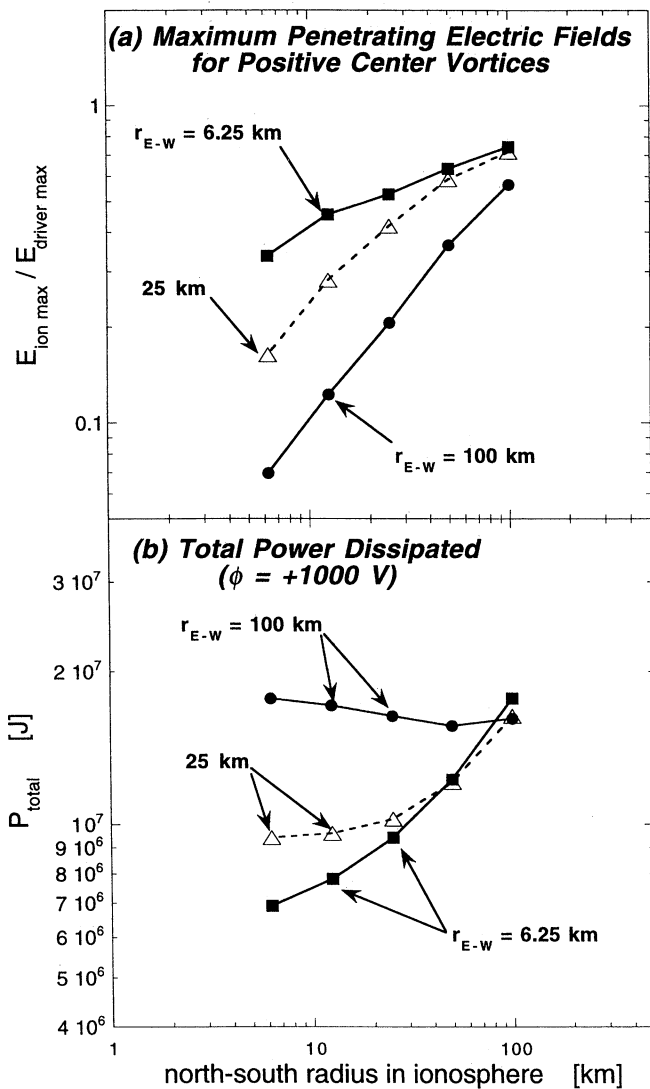$r_{E-W} = 6.25$ km

north-south radius in ionosphere   [km]

Figure 13. For positive center magnetospheric vortices with oval footprints in the ionosphere, (a) the fractional penetration of the vortex electric field down to the ionosphere and (b) the total amount of power dissipated P in the current systems driven by the vortex are plotted as functions of the north-south radius (semiminor or semimajor axis) of the footprint. Three series of curves are run: a series wherein the east-west radius (semimajor or semiminor axis) of the magnetic footprint is 100 km in the ionosphere (circles), a series wherein the east-west radius of the magnetic footprint is 25 km (triangles), and a series wherein the east-west radius of the magnetic footprint is 6.25 km (squares). In each case the potential of the vortex in the magnetosphere is +1000 V.

This proportionality breaks down when the vortex footprint is large, that is, when the power dissipation in the Pedersen currents in the ionosphere begins to become as important as the power dissipation in the upward field-aligned currents. This power dissipation proportional to footprint area can be reasoned as follows. Total power dissipated is, for a fixed voltage generator (here 1000 V), linearly proportional to the total amount of current I flowing through the generator. This amount of current is fixed by the amount of the current driven in the

ionosphere. In the ionosphere, the current density is $j_\perp = \sigma_P E_{ion}$ (see expression (1)). Integrating this in z over the entire ionosphere, one can write $J_\perp = \Sigma_P E_{ion}$, where J is the current per unit horizontal distance across $\vec{E}_{ion}$ and where Σ_P is the height integrated Pedersen conductivity of the ionosphere. The total current flowing in the ionosphere is approximately $I = J_\perp L$, where L is the horizontal scale size of the region of electric field in the ionosphere. For negative center vortices (where the ionospheric electric field is confined to the magnetic footprint), $L \propto r_{foot}$, where r_{foot} is the radius of the ionospheric footprint. Thus $I \propto E_{ion} r_{foot}$. The ionospheric electric field E_{ion} is given by $E_{ion} = f E_{driver}$, where E_{driver} is the strength of the magnetospheric electric field fully mapped down to the ionosphere and f is the fractional mapping of the electric field (e.g., see Figure 4). For a vortex with a fixed potential, the mapped magnetospheric field has $E_{driver} \propto r_{foot}^{-1}$, and from Figure 4 it was found that $f \propto r_{foot}^2$ for negative center vortices with small footprints. Thus, the total current flowing in the ionosphere $I \propto r_{foot}^2$. Since, by current conservation, this equals the current flowing through the generator, the total power dissipated by the fixed-voltage generator is $P \propto r_{foot}^2$, which is P linearly proportional to the area of the footprint in the ionosphere.

In Figure 13 the fractional penetration of the north-south electric field (Figure 13a) and the total power dissipation (Figure 13b) are plotted for positive center vortices with oval footprints. Three different series of vortices are plotted: vortices with east-west footprint radii of 100 km in the ionosphere, vortices with east-west radii of 25 km, and vortices with east-west radii of 6.25 km. In each series the north-south radii of the vortex footprints are varied, and the plots are versus the north-south radius. As can be seen in Figure 13a, the fraction of penetration of the electric field increases as the north-south radius of the vortex footprint increases, as expected. What is perhaps not expected is that the north-south electric fields in the ionosphere are stronger if the east-west extent of the footpoint is narrower; this is seen by looking at the ordering of the three curves in Figure 13a, where the 6.25-km curve is on the top. The reason for this behavior is explored in Figure 14, where the potentials and electric fields for two vortices are plotted: a "wide" vortex that has a footprint that is 200 km wide in the ionosphere and a "narrow" vortex that has a footprint that is 12.5 km wide in the ionosphere, both having footprints with north-south extents of 25 km. As can be seen in the figure (marked as "breakpoint"), the region of downward current, which is the region where $\phi_{ion} = \phi_{mag}$, extends further in the north-south direction in the narrow-east-west case (middle plot) than it does in the wide-north-south case (top plot). This represents a tendency of the downward current region to have a nonzero area, or, more likely, a tendency of the downward current region to have a nonzero circumference (perimeter) through which Pedersen currents can connect. Note that both the wide and the
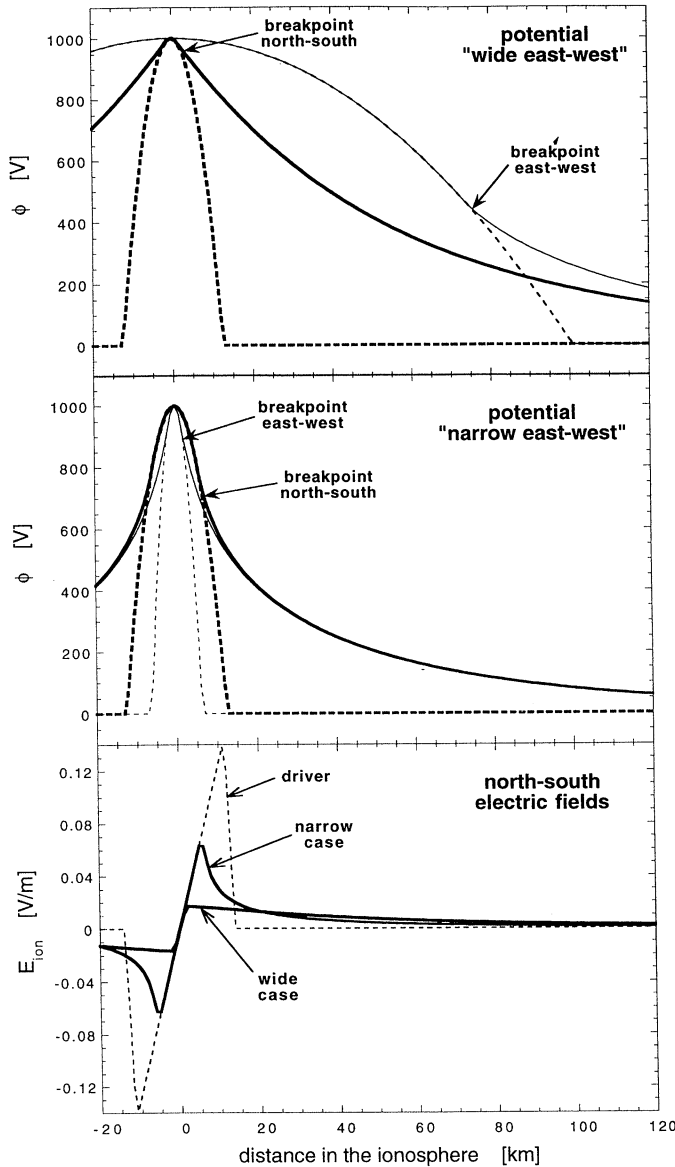
Figure 14. (top and middle) For two positive center vortices with oval magnetic footprints, the electrostatic potential ϕ in the ionosphere is plotted. The vortex of the top plot has a footprint that is wide in the east-west direction and the vortex in the middle plot has a footprint that is short in the east-west direction, with the north-south extents of the footprints being the same for both vortices. (bottom) The north-south electric field in the ionosphere is plotted for both vortices.

narrow vortices have large regions of upward current spreading out beyond the magnetic footprints. In the region of downward current, $\phi_{ion} = \phi_{mag}$ and so also $E_{ion} = E_{driver}$. Since E_{driver} is zero at the center of the vortex and increases with distance outward, if the region of downward current extends further (as it does in the north-south direction in the narrow-vortex case), then the electric field in the ionosphere will be larger.

In Figure 12 the total power dissipated by positive center vortices is plotted as a function of the area of their footprints in the ionosphere (circles). The multi-

ple values obtained for a given area are due to vortices with differing shapes. As can be seen, power dissipation by these fixed-voltage positive center vortices is only slightly dependent on their footprint area. This is very different from the case of negative center vortices, which are plotted as the squares in Figure 12.

4. Flow Channels Coupling to the Ionosphere

In this section the dc electrical coupling of flow channels in the magnetosphere to the ionosphere is examined. A flow channel is taken to be a long region of cross-field flow with a finite width that is confined between semi-infinite regions of no flow. The flow in the channel is associated with an $\vec{E} \times \vec{B}$ drift [e.g., *Borovsky*, 1987; *Galvez*, 1987], and the electric field $\vec{E}$ is confined to the channel. For simplicity, the electric field in the magnetosphere is taken to be uniform within the channel, rapidly dropping to zero at the channel edges. By Coulomb's law $\nabla \cdot \vec{E} = 4\pi n_q$, there is a nonzero charge density n_q at each edge of the flow channel.

In Figure 15 the electric field (top plot) and the electrostatic potential (second plot) for a flow channel coupled to the ionosphere are plotted (solid curves) as functions of distance in the ionosphere across the channel. The magnetospheric (driver) fields and potentials are plotted as the dashed curves. As can be seen in the first and second plots, the driver electric field (electric field of the magnetosphere) resides within the channel, and the electrostatic potential in the magnetosphere corresponding to this electric field has the form of a ramp across the channel. At the high-potential edge of the channel there is a layer of positive charge and at the low-potential edge there is a layer of negative charge. In the second plot of Figure 15 it can be seen that the ramp in the electrostatic potential in the ionosphere is broadened toward the low-potential region compared with the driver potential. Commensurate with this, the electric field in the ionosphere (top plot) is spread outside the magnetic footprint of the channel into the low-potential region. As noted in the figure, outside the footprint the electric field decreases with distance y as $\exp(-y/\ell_\perp)$, where $\ell_\perp = (\Sigma_P/Q_{up})^{1/2} = 79$ km. This spreading of the electric field represents a spreading of the negative charge layer of the flow channel in the ionosphere, while the positive-charge layer remains sharp. The sharpness of the electric-field mapping on the positive-charge side of the flow channel means that the $\vec{E} \times \vec{B}$ drift flow pattern in the ionosphere will be sharp on the positive charge edge, and the spreading of the electric field on the negative-charge side of the flow channel means that the flow pattern in the ionosphere will spread outside the magnetic footprint of the channel on the negative-charge side. In the third plot of Figure 15, the areal power-dissipation rates for the Pedersen and parallel currents are shown. As can be seen, the power dissipated in the Pedersen current oc-

curs across the channel as a Pedersen current flows in the ionosphere between the two charge layers of the flow channel, whereas the parallel power dissipation is concentrated around the negative-charge layer of the flow channel where upward field-aligned current flows. In the bottom two plots of Figure 15 the intensities of the currents are shown. Note the intense spike of downward field-aligned current (magnitude not shown) associated with the positive-charge layer of the channel flow and the broad, weak region of upward field-aligned current around the negative-charge layer of the flow channel. Should the flow velocity of the flow channel be fast enough, then the power dissipated in the parallel current region would be sufficient to result in auroral airglow in the upward field-aligned-current regions. Hence
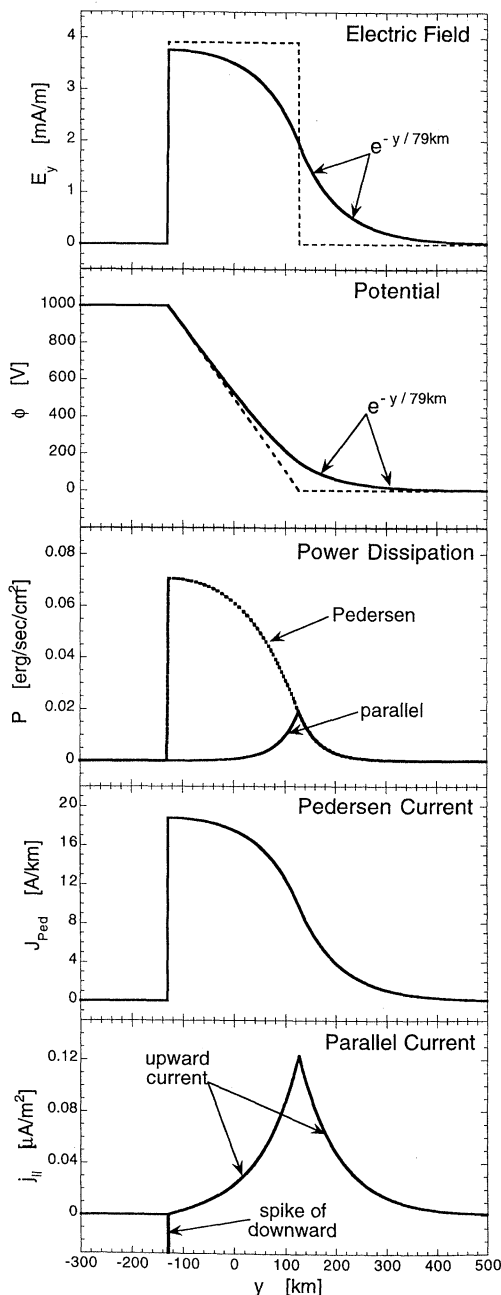
one should expect a broadened region of aurora located around the magnetic footprints of the negative-charged edge of the channel. Observations of flow channels in the ionosphere show aurora on the negative-charge edge [*Sandholt*, 1993; *de la Beaujardiere et al.*, 1994].

In Figure 16 the electric fields are plotted for four cases of channels with footprints of different widths: The dashed curves are the driver electric fields, and the solid curves are the electric fields in the ionosphere. In all cases the electric field is normalized to the value of the driver electric field inside the channel. Full penetration results in an ionospheric electric field with $E/E_{\mathrm{driver}} = 1$. There are several things to note in Figure 16. First, note that when the channel's footprint is narrow, penetration of the electric field from the magnetosphere to the ionosphere is poor, and when the channel footprint is wide, penetration is good. Second, note that the electric field in the ionosphere spreads outside the footprint on the low-potential side of the channel (on the negative-charge side of the channel). Third, note that the region of spreading of the electric field has a characteristic size in the ionosphere (in all cases in Figure 16, $\ell_\perp = (\Sigma_{\mathrm{P}}/Q_{\mathrm{up}})^{1/2} = 79$ km). Fourth, note that the positive-charge edge of the channel remains sharp as it maps down to the ionosphere. Owing to the electric field in the ionosphere, the plasma of the ionosphere $\vec{E} \times \vec{B}$ drifts in the direction of the channel flow in the magnetosphere. In cases where the penetration is not full, there is a slip in the cross-field flow velocity between the magnetosphere and the ionosphere, with the ionosphere lagging the magnetosphere's motion. In all cases, there is some spreading of the electric field as it maps to the ionosphere: This means that the flow channel in the ionosphere is wider than the magnetic footprint of the magnetospheric flow channel. It also means that currents will be driven into the magnetosphere outside of the channel's magnetic footprint, which will produce $\vec{j} \times \vec{B}$ forces in the magnetospheric plasma adjacent to the flow channel.

In Figure 17 the fractional penetration of the flow-channel electric field to the ionosphere is plotted (solid circles) as a function of the width of the magnetic foot-

Figure 15. For a flow channel in the magnetosphere that maps to the ionosphere, a number of quantities are plotted as functions of distance y from a cut through the channel's magnetic footprint in the ionosphere. The channel flow is in the x direction. In the top plot the electric field $E_{\mathrm{y}}(y)$ is shown for the driver (dashed curve) and in the ionosphere (solid curve). In the second plot the electrostatic potential $\phi(y)$ is shown for the driver (dashed curve) and in the ionosphere (solid curve). In the third plot the amount of power dissipation per unit area of the ionosphere $P(y)$ is shown for the upward field-aligned currents (solid curve) and for the Pedersen currents (dotted curve). In the fourth plot the height-integrated Pedersen current density $J_{\mathrm{Ped}}(y)$ is shown (J_{Ped} flows in the y direction). In the bottom plot the field-aligned current density $j_{\|}(y)$ flowing vertically into and out of the ionosphere is shown.
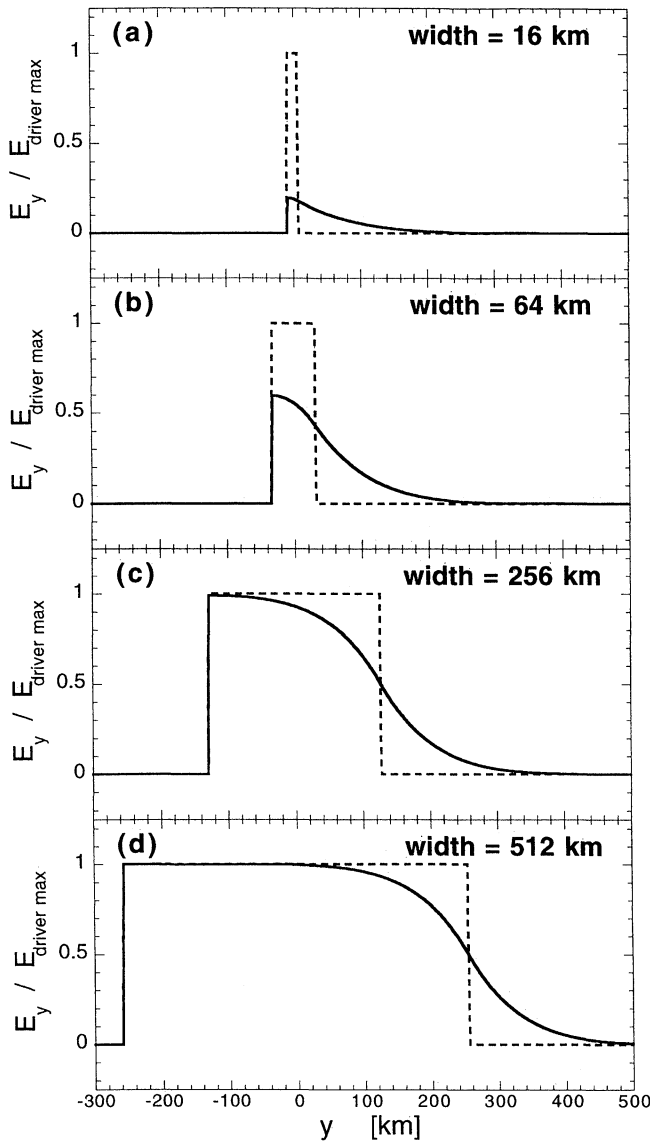
Figure 16. For four magnetospheric flow channels with magnetic footprints that have different widths of (a) 16 km, (b) 64 km, (c) 256 km, and (d) 512 km in the ionosphere, the electric field $E_y(y)$ in the ionosphere and the driver electric field are plotted (solid curves) as functions of distance y in the ionosphere for cuts through the magnetic footprints of the channels. The electric fields in each plot are normalized to the maximum strength of the driver electric field, and also shown (dashed curves) are the normalized driver electric fields.

penetration fraction for flow channels can be expressed as

$$\frac{E_{\text{ion max}}}{E_{\text{driver}}} \approx \left[1 + \left(\frac{d}{\ell_\perp} \right)^{-2} \right]^{-1/2}, \quad (16)$$

which is accurate to within 10% for any value of w. Also plotted in Figure 17 is the fractional penetration of the electric field for positive center vortices (open triangles) and negative center vortices (open circles) as functions of the radius of the vortex footprint in the ionosphere. Note that for small footprints, the penetration fraction for the flow channels lies in between the penetration fractions for positive and for negative vortices.

In Figure 18 the current system driven by a flow channel is sketched. The top of the sketch represents the magnetosphere and the bottom represents the iono-
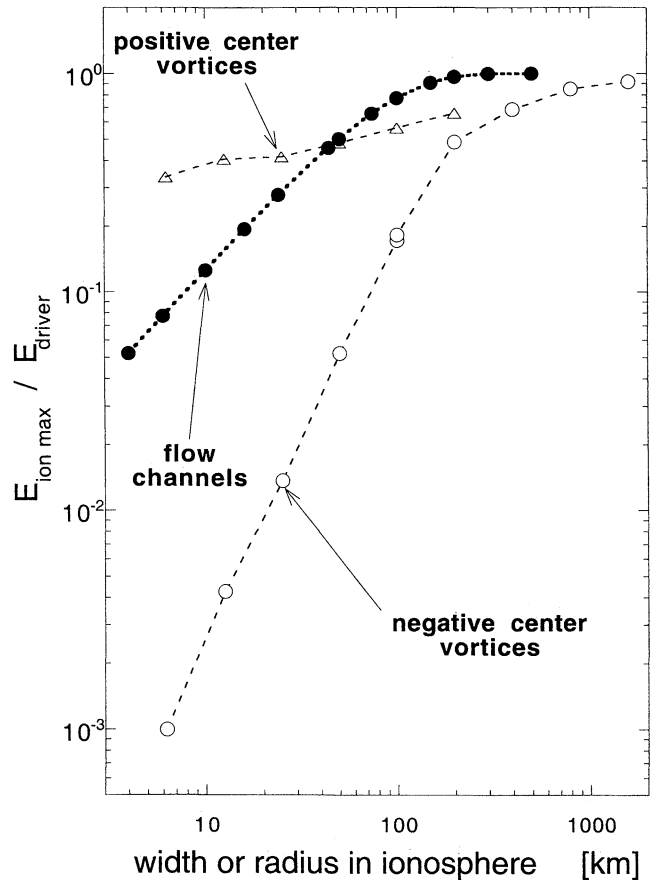

Figure 17. For magnetospheric flow channels that have differing widths of their magnetic footprints in the ionosphere, the fractional penetration of the channel electric field down to the ionosphere is plotted (solid circles) as a function of the footprint width. The fractional penetration is taken to be the ratio of the maximum electric field that appears in the ionosphere divided by the driver electric field strength. Also plotted are the fractional electric-field penetration for positive center vortices in the magnetosphere (triangles) and the fractional electric-field penetration for negative center vortices in the magnetosphere (open circles). The vortices here are idealized to have circular footprints, and the fractional penetration is plotted as a function of the footprint radius in the ionosphere.
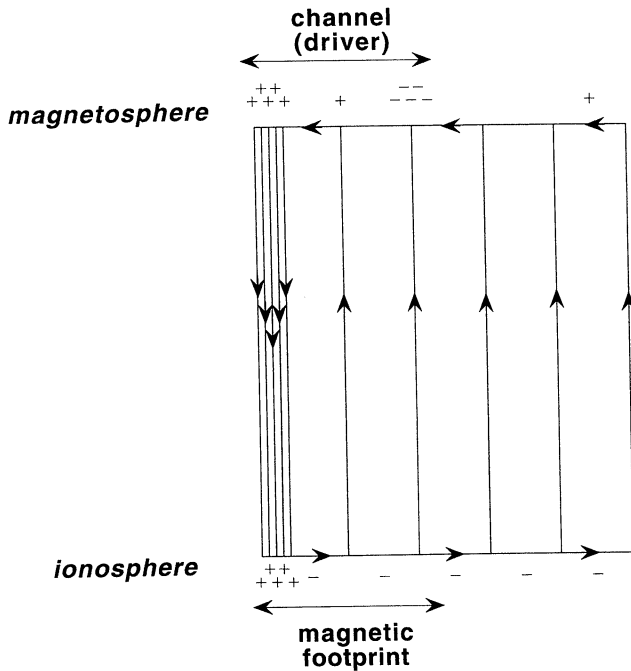
print of the channel in the ionosphere. This fractional penetration is expressed as $E_{\text{ion max}}/E_{\text{driver}}$, where E_{driver} is the strength of the driver electric field (the full magnetospheric electric field if it would be magnetically mapped into the ionosphere) and $E_{\text{ion max}}$ is the maximum value of the electric field that appears in the ionosphere. Here, $\ell_\perp = (\Sigma_P/Q_{\text{up}})^{1/2} = 79$ km. Note that if the width of the channel footprint is large compared with $\ell_\perp$, the mapping is full (i.e., $E_{\text{ion max}} \approx E_{\text{driver}}$), and if the width w of the channel footprint is $w \ll \ell_\perp$ then $E_{\text{ion max}}/E_{\text{driver}} \approx w/\ell_\perp$. For any value of w, the

**channel
(driver)**

magnetosphere

ionosphere

**magnetic
footprint**

Figure 18. A sketch of the current system driven by a flow channel in the magnetosphere. Note that the convergence of the magnetic field lines between the magnetosphere (top) and the ionosphere (bottom) is not depicted in the sketch. Note that the currents spread outside of the magnetic footprint of the channel on the negative-charge side (low-potential side) of the channel.

sphere; the convergence of the magnetic field lines in mapping from the magnetosphere to the ionosphere is not depicted in the sketch. The width of the channel in the magnetosphere is noted at the top of the figure and the width of the channel's magnetic footprint in the ionosphere is noted in the bottom of the figure. The currents are indicated as the solid lines with arrowheads denoting the direction of current flow. A downward field-aligned current flows from the positive edge of the channel in the magnetosphere down to the ionosphere. This downward current is narrow and strong. A broad region of weaker upward field-aligned current forms around the negative-charge edge of the channel, spreading outside the channel itself. This current flows in the region where $\phi_{ion} > \phi_{mag}$ (cf. Figure 15). The field-aligned currents close across $\vec{B}$ in the ionosphere as Pedersen currents, and they close in the flow channel in the ionosphere as polarization-drift currents [e.g., Borovsky, 1987, 1992]. The $\vec{j} \times \vec{B}$ forces for these closure currents act to brake the motion inside the magnetospheric flow channel and act to transfer its momentum to the ionosphere (through collisions to the neutral gas). Owing to the spreading of the current system on the negative-charge edge of the channel, a region of reversed flow will be produced in the magnetosphere adjacent to the negative-charge edge of the channel.

5. The Effects of Resistivity in the Downward Current Regions

So far in this paper it has been assumed that the regions of downward field-aligned current have infinite conductivity (e.g., that $Q_{down} = \infty$, see Figure 1), that is, that $\phi_{mag} = \phi_{ion}$ in these regions (e.g., expression (9)). For some time there has been evidence that the downward current regions of the aurora have nonzero potential drops, that is, that those regions do not have infinite parallel conductivity. Just as the upward current regions of the aurora with their field-aligned potential drops are characterized by downgoing electron beams, upgoing electron beams have been associated with regions of downward field-aligned current [Klumpar and Heikkila, 1982; Hultqvist et al. 1988; Boehm et al., 1995; Elphic et al., 1998; Carlson et al., 1998], implying field-aligned potential drops. Such auroral electron beams have been observed in the magnetosphere for decades [McIlwain, 1975; Klumpar et al., 1988], and surveys of these populations indicate that they are common in the auroral zone [Collin et al., 1982; Klumpar, 1993], although the interpretation of potential drops in the downward current regions has remained controversial.

In this section the infinite-conductivity assumption $Q_{down} = \infty$ (expression (9)) for the downward current regions will be replaced with a Knight-type relation

$$j_{\parallel} = Q_{down} \left(\phi_{mag} - \phi_{ion} \right), \qquad (17)$$

with $\phi_{mag} \geq \phi_{ion}$ (see also Chiu et al. [1981]). The new assumption is that the downward current regions are Ohmic, that is, $j_{\parallel} \propto \Delta\phi_{\parallel}$. As of yet, there is insufficient information to determine a current-voltage relation for the downward current regions of the aurora [e.g., Elphic et al., 1998]; rather than an Ohmic relation $\Delta\phi \propto j$, a Child-Langmuir relation $\Delta\phi \propto j^{2/3}$ [e.g., Chen, 1965] or a strong-double-layer relation with $\Delta\phi$ independent of j [Block, 1978; Carpenter and Torven, 1987] might just as well be taken. For the purpose of the present study, the desire is to merely break the infinite-conductivity assumption and to note the gross effects that result. Quantitative studies of the changes in the power dissipation, etc., caused by relaxing this assumption cannot at this stage be taken too seriously, since an appropriate current-voltage relation for the downward current regions cannot be guessed at. In this section the effects of the relaxation of the infinite-conductivity assumption will be examined for the mapping of vortices and for flow channels.

The effect is easiest seen on the mapping of magnetospheric flow channels into the ionosphere. In Figure 19 the electric field (top plot) and electrostatic potential (bottom plot) are shown for a cut through a flow channel that is mapped down from the magnetosphere for three cases: $Q_{down} = \infty$, $Q_{down} = 10\,Q_{up}$, and $Q_{down} = Q_{up}$. The driver electric field and driver potential
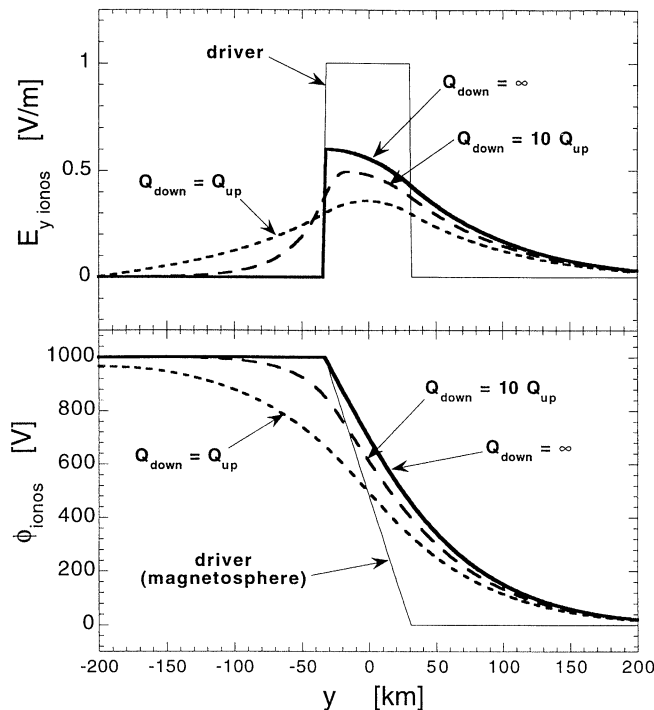
Figure 19. A magnetospheric flow channel is run for three cases: a case where the downward current regions are infinitely conducting ($Q_{down} = \infty$), a case where the downward current regions are 10 times more conducting than the upward current regions ($Q_{down} = 10\ Q_{up}$), and a case where the downward current regions have the same conductivity as the upward current regions ($Q_{down} = Q_{up}$). For cuts through the channel's magnetic footprint in the ionosphere, (top) the electric field E_y in the ionosphere and (bottom) the electrostatic potential ϕ are plotted. Also plotted are the driver electric field and driver potential.

are plotted as the fine solid curves, the mapped electric field and mapped potential for the $Q_{down} = \infty$ case are plotted as the bold solid curves, the mapped electric field and mapped potential for the $Q_{down} = 10\ Q_{up}$ case are plotted as the long-dashed curves, and for the $Q_{down} = Q_{up}$ case they are plotted as the short-dashed curves, As can be seen by comparing the bold solid curves with the dashed curves, relaxing the $Q_{down} = \infty$ condition results in a spreading of the positive charge layer on the high-potential edge of the flow channel. In the $Q_{down} = 10\ Q_{up}$ case, the spreading of the positive-charge layer is not as large as the spreading of the negative-charge layer. However, in the $Q_{down} = Q_{up}$ case the positive-charge layer spreads as much as the negative-charge layer does, and the electric-field and potential curves become symmetric across the channel for this case.

In Figure 20 the electric fields of circular vortices mapped to the ionosphere are plotted; Figure 20a is for a set of positive center vortices, and Figure 20b is for a set of negative center vortices. Note that there is a difference in vertical scale between the two graphs. In both plots the driver electric field is shown as the dashed curve, and the three solid curves are the magne-

tospheric electric field mapped to the ionosphere for the three cases $Q_{down} = \infty$, $Q_{down} = 10\ Q_{up}$, and $Q_{down} = 1\ Q_{up}$. In Figure 20a a comparison of the driver electric field with the "∞:1" electric field shows a full mapping of the electric field at the center of the vortex (where there is positive charge) and a spreading of the negative-charge region on the outside of the vortex. Comparing the "10:1" and the "1:1" curves with these, it can be seen that a relaxation of the $Q_{down} = \infty$ condition results in an incomplete mapping of the electric field in the positive-charge region in the center of the vortex. Similar phenomena are seen for the negative center vortices in Figure 20b. A comparison of the driver electric field and the "∞:1" curve shows that the positive-charge region on the outer edge of the vortex maps down sharply. Then comparing the "10:1" and the "1:1" curves with these shows that relaxing the $Q_{down} = \infty$ condition results in a spreading of the positive charge region. Note that for both the positive center vortices and the negative center vortices, relaxing the $Q_{down} = \infty$ condition results in weaker electric fields in the ionosphere.

In Figure 21 the electrostatic potentials ϕ in the ionosphere of a number of vortices with elliptical footprints are plotted. The vortices in Figure 21a are positive center vortices, and those in Figure 21b are negative center vortices. The top plot in each of Figures 21a and 21b depicts the driver potential, the second plot depicts the mapping with $Q_{down} = \infty$, the third plot depicts the mapping with $Q_{down} = 0.1\ Q_{up}$, and the bottom plots depict the mapping with $Q_{down} = Q_{up}$. As can be seen in the second plots of Figures 21a and 21b, for $Q_{down} = \infty$ the negative center vortex is confined to its footprint, and the positive center vortex spreads outside of its magnetic footprint (particularly in the narrow north-south direction). Also, the full potential of the 1000-V driver reaches the ionosphere for the positive center case and only a small fraction of the 1000-V driver reaches the ionosphere for the negative center case. As can be seen in the third and bottom plots, these trends are broken when Q_{down} is finite. The fact that the negative center vortex is no longer confined to the magnetic footprint is easily seen by comparing the various plots in Figure 21b. The fact that the full potential of the driver no longer reaches the ionosphere is easily seen by comparing the various plots in Figure 21a. Also note in Figure 21b that the fraction of the driver potential that penetrates to the ionosphere for negative center vortices increases as Q_{down} is lowered. Note also, although it is difficult to see owing to the differences in vertical scales between the left-hand and right-hand columns, the potential profiles $\phi(x, y)$ in the $Q_{down} = Q_{up}$ cases in the two bottom plots are identical except for a change of sign on ϕ.

In each of the plots of Figure 21, the total power dissipation P in the current systems driven by the magnetospheric vortices is indicated. Note in Figure 21a that reducing Q_{down} down from ∞ greatly reduces the total
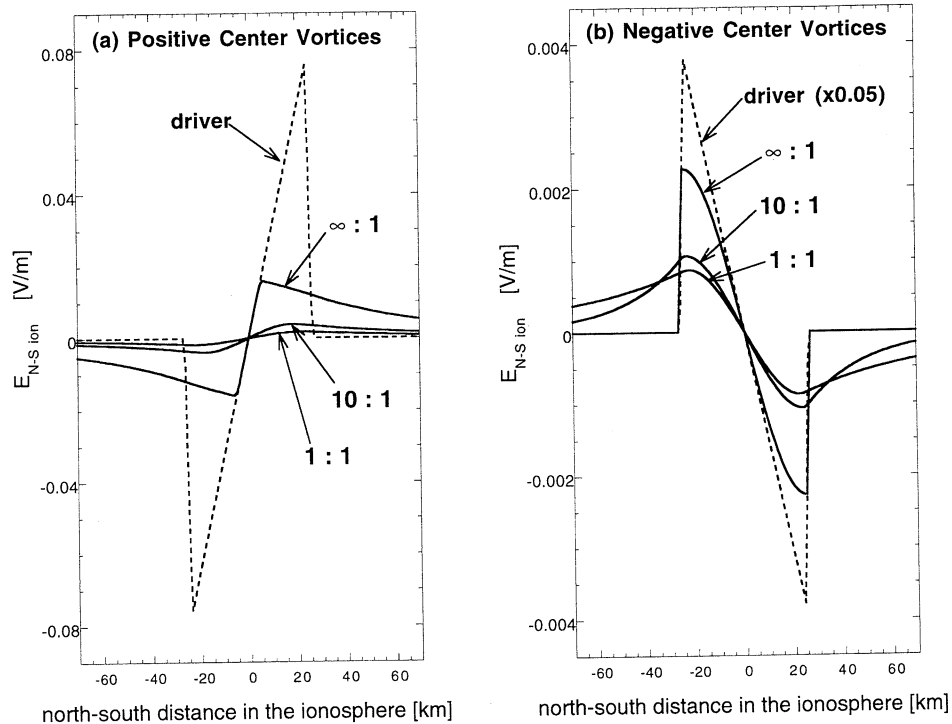
Figure 20. (a) A positive center magnetospheric vortex and (b) a negative center magnetospheric vortex are each run for three cases: a case where the downward current regions are infinitely conducting ($Q_{down} = \infty$, denoted as "∞:1"), a case where the downward current regions are more conducting than the upward current regions ($Q_{down} = 10\ Q_{up}$, denoted as "10:1"), and a case where the downward current regions have the same conductivity as the upward current regions ($Q_{down} = Q_{up}$, denoted as "1:1"). These vortices are idealized to have circular magnetic footprints in the ionosphere. For north-south cuts through the footprint in the ionosphere, the north-south component of the electric field E in the ionosphere is plotted. Also plotted is the driver electric field.

power dissipation of the positive center vortices. This means that the positive center vortices do not drive the strong current systems when the infinite-conductivity condition for the downward currents is relaxed. Note in Figure 21b that reducing Q_{down} down from ∞ does not strongly affect the total power dissipation of the negative center vortices. This means that the coupling of the negative center vortices to the ionosphere is not strongly affected by relaxing the infinite-conductivity condition for the downward currents.

6. Example Vortices

As an application of these results, the coupling to the ionosphere of two hypothetical vortices in the magnetosphere is examined. The two vortices are identical, except that one is positive centered ($\vec{\Omega}$ antiparallel to $\vec{B}$) and the other is negative centered ($\vec{\Omega}$ parallel to $\vec{B}$). The magnetospheric vortices are taken to be centered at $X = -20\ R_E$, $Y = 0$ in the magnetotail, as sketched in the top diagram of Figure 22, and the parameters of the vortices are listed in Table 2. The vortices are taken to be circular in the equatorial plane of the magnetotail, with a radius $r_{vortex} = 0.8\ R_E$, which gives a flow vortex with diameter 1.6 R_E, which matches the ap-

proximate mixing length of the flow turbulence in the magnetotail plasma sheet 20 R_E downtail [*Borovsky et al.*, 1997]. With the view of Figure 22 (looking down from the north), a positive center vortex corresponds to a clockwise flow in the magnetotail, and a negative center vortex corresponds to a counterclockwise flow in the magnetotail. For simplicity, the vortex is taken to have solid-body rotation in the magnetosphere. The maximum rotation velocity, which occurs at the outer edge of the vortex, is taken to be 150 km/s, which is twice the rms flow velocity for the turbulence observed by ISEE 2 in the magnetotail [e.g., *Borovsky et al.*, 1997, Table 1]).

The shape and size of the magnetic footprint of such a vortex are estimated by tracing magnetic field lines from the magnetotail to the ionosphere with both the T89c [*Tsyganenko*, 1989; *Peredo et al.*, 1993] and T96 [*Tsyganenko*, 1996] magnetic field models. In the top diagram of Figure 22 the position and size of the vortex in the plasma sheet are shown with a bird's-eye view of the Earth and vortex in the $X - Y$ plane. In the bottom diagram of Figure 22 the magnetic footprint of the vortex in the ionosphere is shown in north-south versus east-west coordinates according to the field-line tracing in both the T89c and T96 models. (The north-south dis-
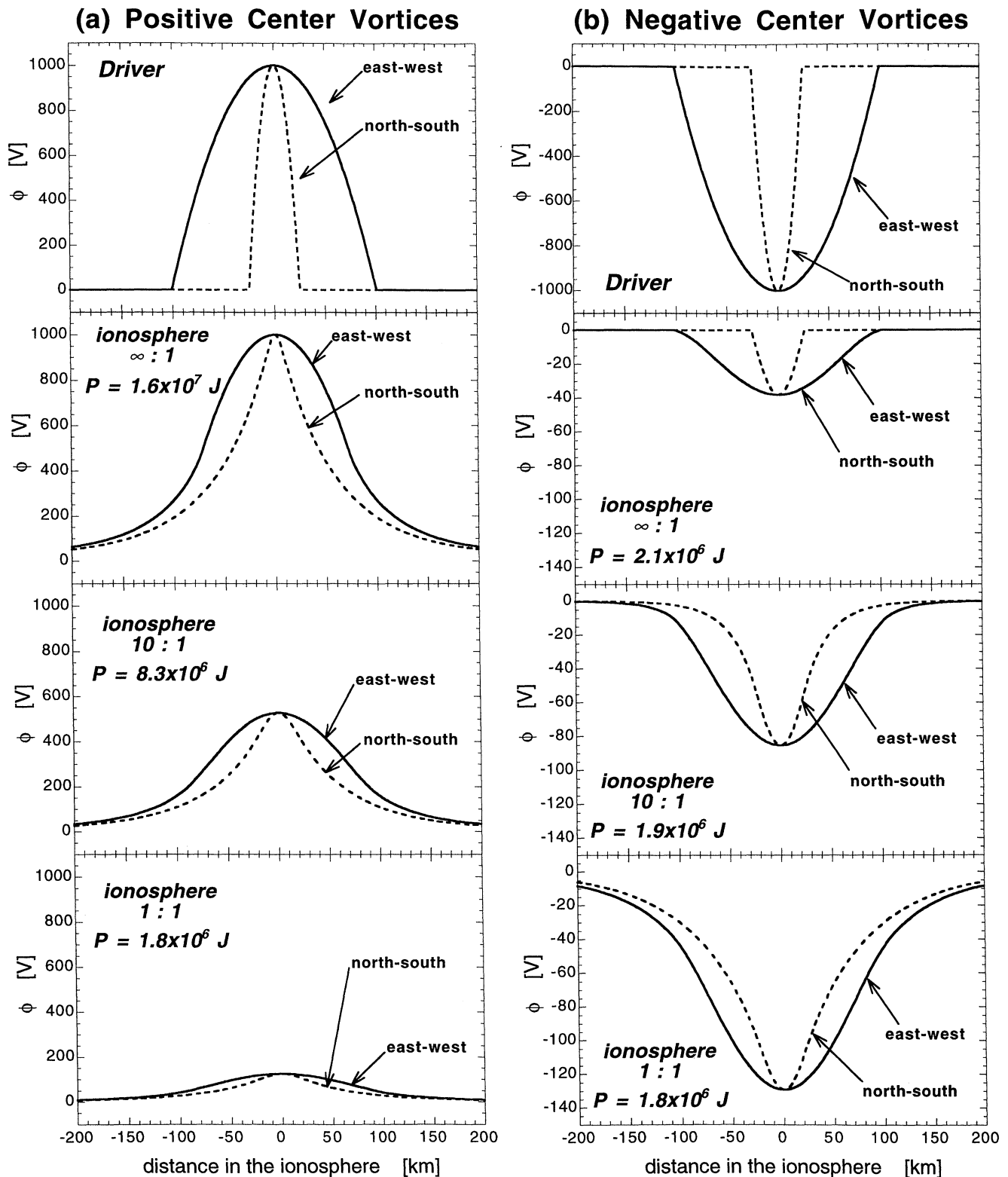
(a) Positive Center Vortices

(b) Negative Center Vortices

Figure 21. (a) For a positive center magnetospheric vortex with an oval magnetic footprint in the ionosphere and (b) for a negative center magnetospheric vortex with an oval magnetic footprint in the ionosphere, the coupling to the ionosphere is calculated for three cases: a case where the downward current regions are infinitely conducting ($Q_{down} = \infty$, denoted as "∞:1"), a case where the downward current regions are more conducting than the upward current regions ($Q_{down} = 10\ Q_{up}$, denoted as "10:1"), and a case where the downward current regions have the same conductivity as the upward current regions ($Q_{down} = Q_{up}$, denoted as "1:1"). In each plot the electrostatic potential ϕ in the ionosphere is shown for an east-west cut through the center of the footprint (solid curves) and for a north-south cut (dashed curves). The top plots show the driver electrostatic potential for the two cuts. The total power dissipation in the driven current systems is indicated for each plot.
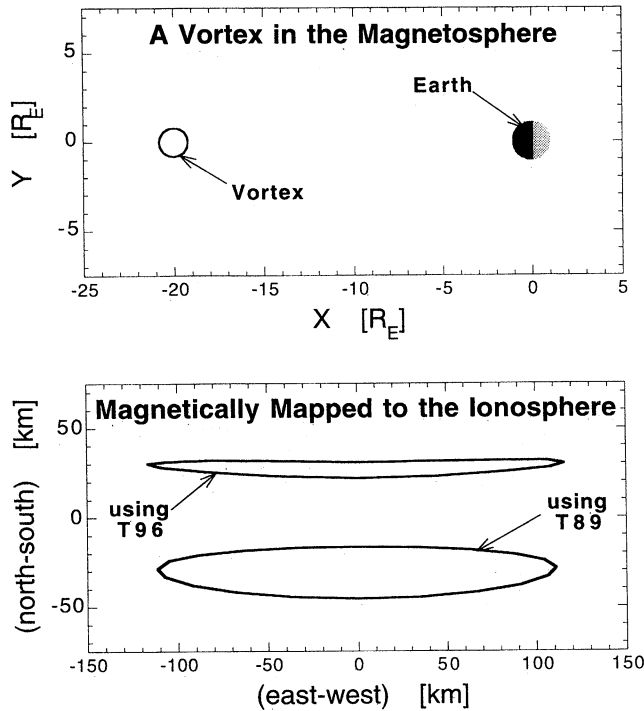
A Vortex in the Magnetosphere

Magnetically Mapped to the Ionosphere

Figure 22. (top) A sketch of the Earth and a vortex in the center of the magnetotail as viewed from high above the north pole. The center of the vortex is located at $X = -20$ R_E, $Y = 0$ and the vortex has a radius of 0.8 R_E. (bottom) The magnetic footprint of the vortex is plotted in the ionosphere, where the footprint was determined by tracing a number of magnetic field lines that threaded the perimeter of the magnetospheric vortex from the vortex to the Earth. The Tsyganenko T89c and T96 magnetic field models were used. The north-south displacement of the footprints obtained from the two models is arbitrary.

placement of the two patterns is arbitrary here.) Both magnetic field models indicate that the circular vortex in the magnetotail maps to a narrow east-west-aligned shape in the ionosphere (see also *Kaufmann et al.* [1990]). For the parameters used for the field models, the T89c mapping yields a 29-km by 222-km footprint and the T96 mapping yields a 8.9-km by 232-km footprint. Values between these two sets will be taken for the example vortices: a footprint that has a major axis that is 230 km long in the east-west direction and a minor axis that is 20 km wide in the north-south direction (see Table 2).

The strength of the magnetic field in the vortex in the magnetosphere at 20 R_E downtail is taken to be 2.3 nT $= 2.3 \times 10^{-5}$ G. This value is obtained from flux conservation as the 0.8-R_E-radius vortex in the magnetosphere maps to a 20-km by 230-km spot in the ionosphere where the magnetic field strength is 0.5 G. The value 2.3 nT at 20 R_E downtail is consistent with values that are typical in the T89c and T96 models in the neutral sheet, as can be seen in Figures 4 and 5 of *Borovsky et al.* [1998]. Note, however, that *Borovsky et al.* [1998] pointed out that the values of B in the

neutral sheet in these models are smaller than values that are measured there by ISEE 2 (also Figures 4 and 5 therein). If the true value of B in the magnetotail is larger than the model values, then the amount of magnetic flux threading the vortex in the magnetosphere would be larger, and so the true footprint of a vortex in the ionosphere would be larger than 230 km by 20 km in the ionosphere.

With a magnetic-field strength of 2.3 nT and a maximum flow velocity of 150 km/s in the example vortices in the magnetosphere, the maximum electric-field strength in the vortices is $E_{max} = 0.34$ mV/m (as noted in Table 1). Since the example vortices are taken to have solid-body-rotation flow patterns, the electric fields are zero at the vortex centers and linearly increase in magnitude with radius out to the maximum value of 0.34 mV/m at the outer edge of the vortex. Integrating the solid-body-rotation electric field across the vortices from their centers to their edges yields electrostatic potentials of ± 856 V for the example vortices. If the elec-
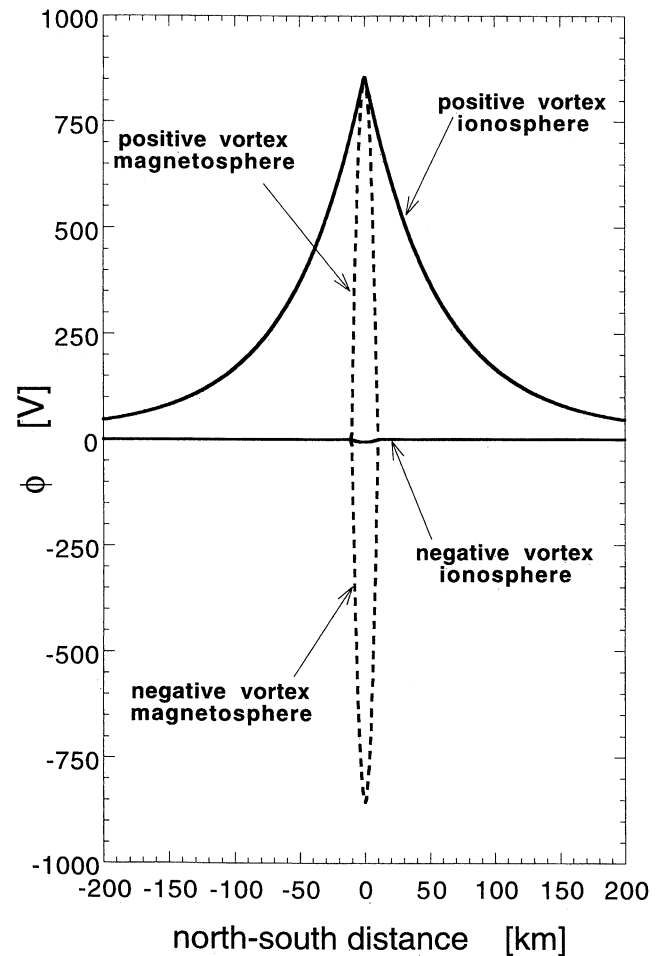

Figure 23. For the example positive center vortex and the example negative center vortex contained in Table 2, the electrostatic potential ϕ is plotted (solid curves) for north-south cuts through the center of the magnetic footprints in the ionosphere. Also plotted (dashed curves) is the driver potential for each vortex.

Table 2. Parameters and Results for Example Vortices

Parameter	Positive center Vortex	Negative center Vortex
>Magnetosphere<		
r_{vortex}	0.8 R_E	0.8 R_E
B	2.3×10^{-5} G	2.3×10^{-5} G
v_{max}	150 km/s	150 km/s
E_{max}	0.34 mV/m	0.34 mV/m
ϕ_{max}	+856 V	-856 V
>Ionosphere<		
Σ_P	5 ohm^{-1}	5 ohm^{-1}
Q_{up}	8×10^{-10} ohm^{-1}m^{-2}	8×10^{-10} ohm^{-1}m^{-2}
footprint	20 km $\times$ 230 km	20 km $\times$ 230 km
B	0.5 G	0.5 G
$\Delta\phi$	856 V	6.4 V
$E_{\text{N-S max}}$	13.8 mV/m	0.88 mV/m
$E_{\text{E-W max}}$	11.2 mV/m	0.084 mV/m
$v_{\text{E-W max}}$	276 m/s	17.6 m/s
$j_{\parallel\text{up max}}$	0.38 μA/m^2	0.46 μA/m^2
$J_{\text{Ped max}}$	4.4 A/km	0.069 A/km
$E_{\text{max}}/E_{\text{driver}}$	9.1%	0.58%
P_{total}	1.39×10^7 W	7.13×10^5 W
$P_{\text{ionos}}/P_{\text{total}}$	69.3%	0.63%
$P_{\text{parallel}}/P_{\text{total}}$	30.6%	99.4%

trostatic potential is defined to be at zero outside the example vortices where the electric field is zero, then the center of the positive center vortex is at +856 V and the center of the negative center vortex is at -856 V.

Expressions (8) and (9) are computationally solved to obtain solutions to expression (7) for the two example vortices: These solutions are displayed in Figures 23-27. The potentials are plotted in Figure 23 for cuts in the north-south direction (in the ionosphere) through the two vortices. The driver (magnetospheric) potentials are plotted as the dashed curves and the potentials in the ionosphere are plotted as the solid curves. As expected, the total potential difference of 856 V reaches the ionosphere for the positive center vortex, but only 6.4 V of potential difference reaches the ionosphere for the negative center vortex (see Table 2). Also, as expected, the potential pattern spreads outside of the 20-km magnetic footprint for the positive center vortex,

and the pattern is confined to within the 20-km footprint for the negative center vortex.

In Figure 24 the east-west flow velocity ($\vec{E} \times \vec{B}$) in the ionosphere is plotted as a function of the north-south distance in the ionosphere for cuts through the two example vortices. As can be seen, the plasma flows in the ionosphere are much stronger and are over a much broader north-south region for the positive center vortex than for the negative center vortex. Basically, a positive center vortex electrically connects to the ionosphere better than does a negative center vortex. As noted in Table 2, the maximum east-west flow velocity in the ionosphere is 276 m/s for the positive center vortex and is 17.6 m/s for the negative center vortex. Note in Figure 24 that the sense of rotation in the ionosphere differs for the negative center and positive center vortices, as it does in the magnetosphere.

In Figure 25, two-dimensional plots of the $\vec{E} \times \vec{B}$ drift velocity in the ionosphere are shown. Figure 25a is for
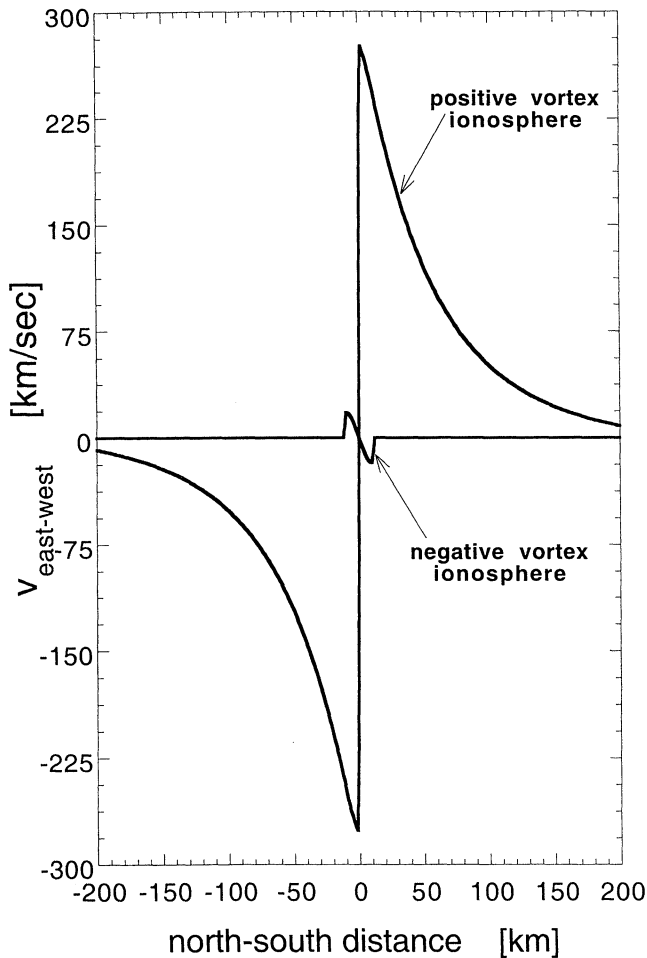
Figure 24. For the example positive center vortex and the example negative center vortex contained in Table 2, the east-west component of the $\vec{E} \times \vec{B}$ drift velocity $v_{\text{east-west}}$ in the ionosphere is plotted for north-south cuts through the centers of the magnetic footprints.

Pedersen current density J_{Ped} with units of A/km. The downward field-aligned currents (negative values) are strong and are confined to small regions: the center of the vortex for the positive center vortex, and the outer edge of the vortex for the negative center vortex. In Figure 26a it can be seen that the region of upward field-aligned current is broad (recall that the magnetic footprint of the vortex only extends to ± 10 km in the north-south direction in the ionosphere). Similarly, the
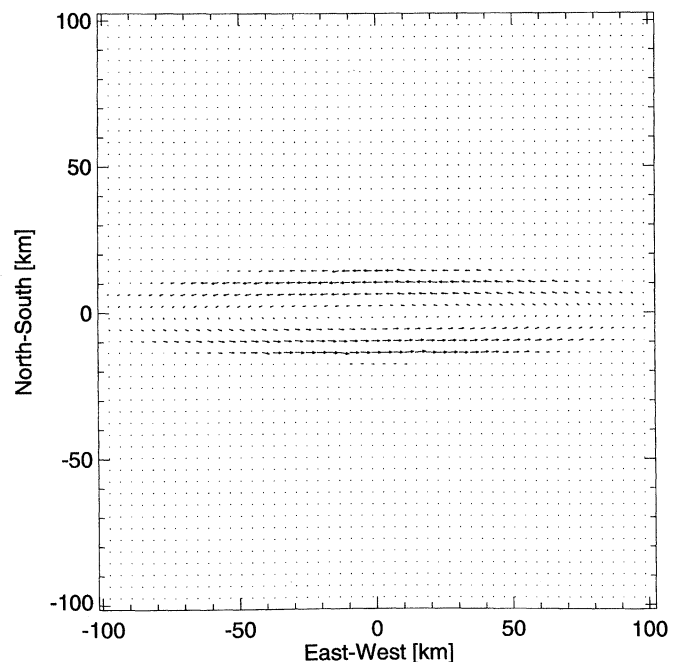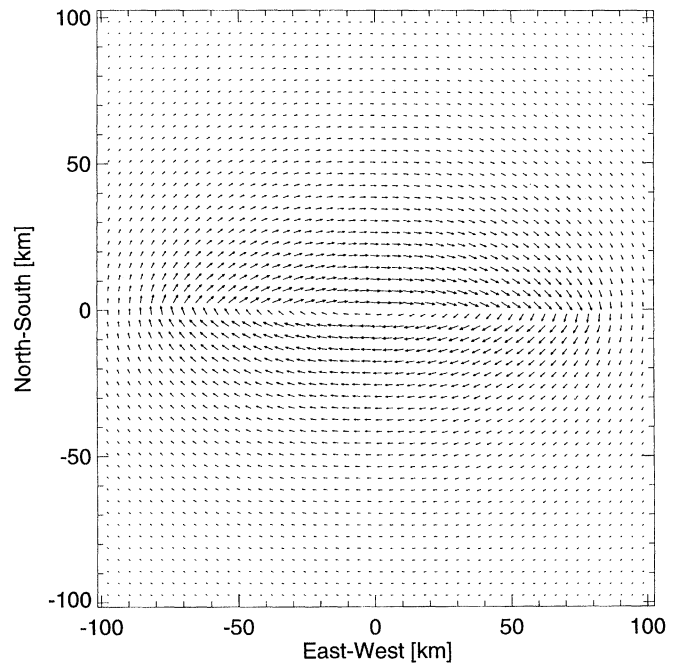
the mapping of the positive center vortex into the ionosphere and Figure 25b is for the mapping of the negative center vortex; in Figure 25a the arrow length is 200 m/s per cell length and in Figure 25b the arrow-length normalization is 20 m/s per cell length. As the flow arrows show, the flow pattern in the ionosphere is greatly broadened outside the magnetic footprint for the positive center vortex, whereas the flow pattern is confined to the magnetic footprint for the negative center vortex. Note that the flow pattern in the ionosphere is quasi-circular for the positive center vortex, and the flow-pattern is greatly east-west aligned for the negative center vortex. Note also the difference in the sense of rotation of the two flow patterns.

In Figure 26 the parallel and Pedersen currents are plotted for north-south cuts in the ionosphere through the positive center vortex (Figure 26a) and the negative center vortex (Figure 26b). Note that the left-hand axis and the solid curves pertain to the parallel current density $j_{\parallel}$ with units of $\mu A/m^2$ and that the right-hand axis and the dashed curves pertain to the height-integrated

Figure 25. For (a) the example positive center vortex and (b) the example negative center vortex contained in Table 2, two-dimensional vector plots of the $\vec{E} \times \vec{B}$ drift velocity in the ionosphere are constructed.
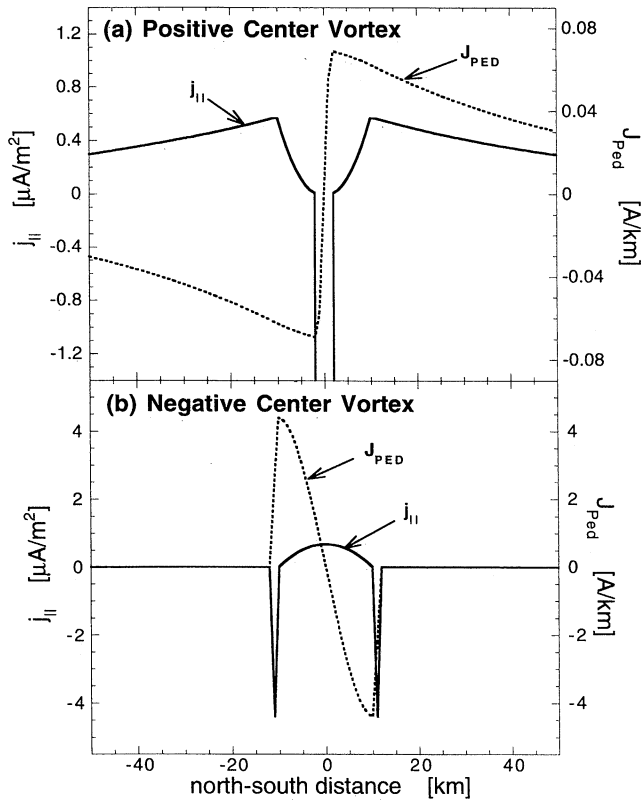
Figure 26. For (a) the example positive center vortex and (b) the example negative center vortex contained in Table 2, the field aligned current density $j_{\|}$ (solid curves and left-hand axis) and the height-integrated Pedersen current density J_{Ped} (dashed curves and right-hand axis) are plotted for north-south cuts through the centers of the magnetic footprints in the ionosphere. The sign of $j_{\|}$ is positive for upward field-aligned currents and negative for downward field-aligned currents.

region of Pedersen current, which connects to the field-aligned current, is also broad, extending well outside of the magnetic footprint of the negative center vortex. In Figure 26b it can be seen that the parallel and Pedersen currents are confined to the magnetic footprint of the positive center vortex. As can be seen from Figure 26 and from Table 2, the maximum values of the upward field-aligned current density into the ionosphere are similar for the two vortices, but the Pedersen linear current densities in the ionosphere are much stronger for the positive center vortex than for the negative center vortex.

In Figure 27 the power dissipated per unit area of the ionosphere is plotted for north-south cuts through the center of the positive center vortex (Figure 27a) and through the center of the negative center vortex (Figure 27b). The power dissipated $Q_{\mathrm{up}} \, (\phi_{\mathrm{ion}} - \phi_{\mathrm{mag}})$ in the upward field-aligned currents is plotted as the solid curves and the power dissipated $\Sigma_{\mathrm{P}} E_{\mathrm{ion}}^2$ in the Pedersen currents is plotted as the dashed curves. In particular, if the voltage difference between the magnetosphere and the ionosphere gets to be large (kV or more), the en-

ergy dissipated in the upward field-aligned currents will go into downward electron acceleration, which will be converted (partially) to auroral airglow in the upper atmosphere. As a rule of thumb, 0.5 erg s^{-1} cm^{-2} of electron flux into the atmosphere will produce about 1 kR (kilorayleigh) of visible emission [e.g., *Dalgarno et al.*, 1965, Table 1 or *Meier and Strickland*, 1991, Table 1], which is about the threshold of visibility to the naked eye. As can be seen in Figure 27, the example positive center vortex has a large region (extending well outside the magnetic footprint) that is just below visible, and the example negative center vortex has a small region (confined inside the magnetic footprint) that is just about visible. Note that the positive center vortex has a large region of strong power dissipation in the Pedersen currents. The power dissipation in the Pedersen currents goes into ion heating and into heating the neutral atmosphere and does not lead to aurora.

In Figure 28, two-dimensional contour plots are made of the logarithm of the power dissipated per unit area in the upward field-aligned currents for the two example
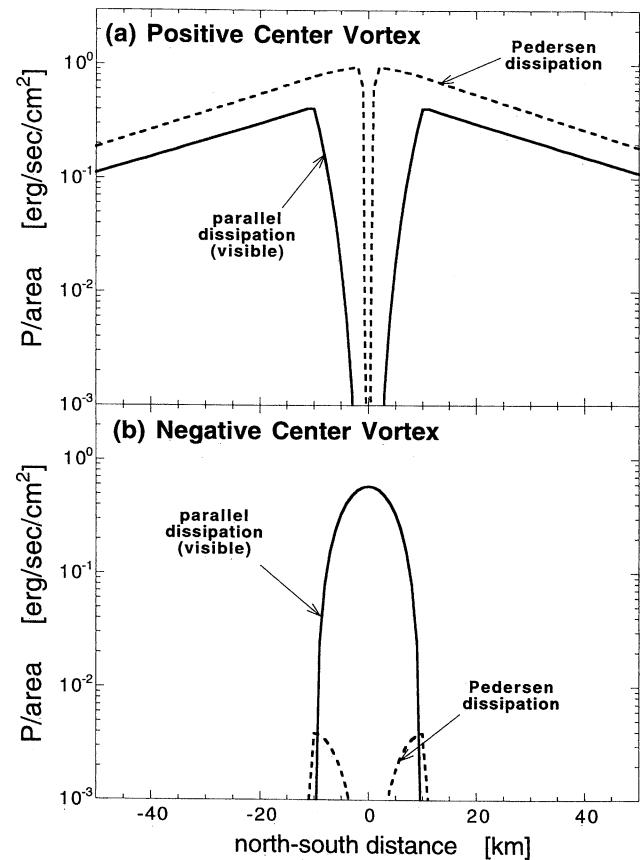

Figure 27. For (a) the example positive center vortex and (b) the example negative center vortex contained in Table 2, the power dissipation per unit area of the ionosphere P is plotted for north-south cuts through the centers of the magnetic footprints in the ionosphere. The solid curves are the power dissipation in (upward) field-aligned currents, and the dashed curves are the power dissipation in Pedersen currents.
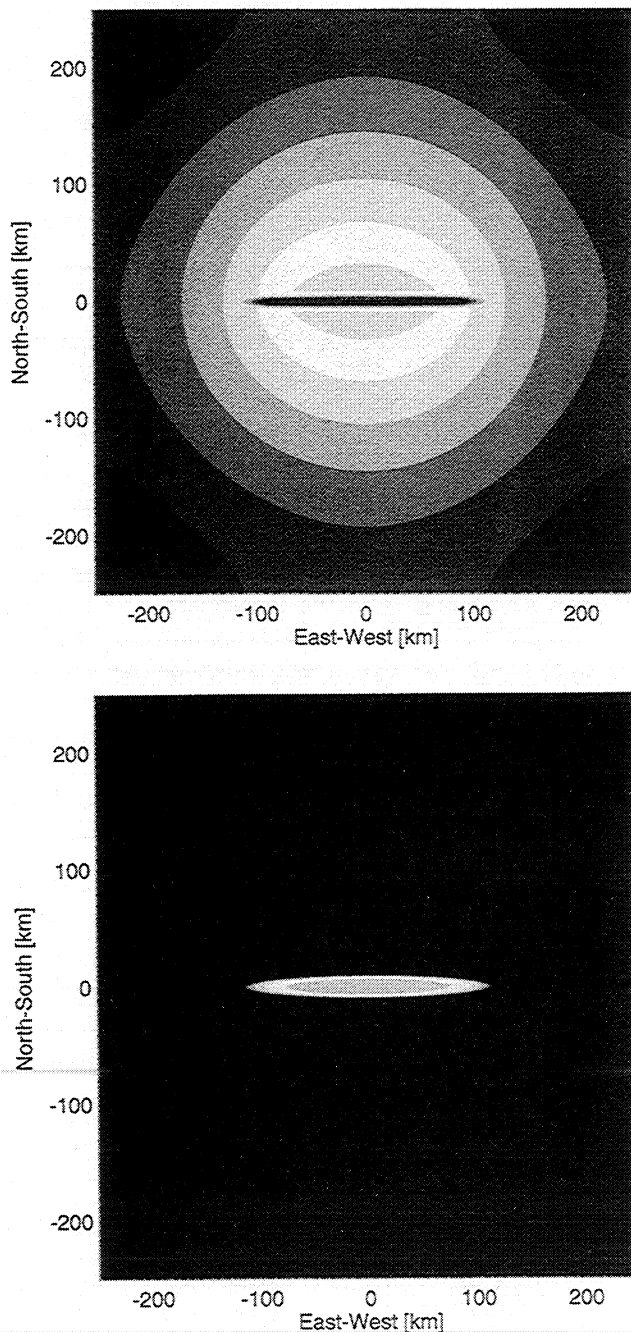
at intensities that are visible to the naked eye. In such cases the auroral patterns would look like the gray-scale patterns plotted in Figure 28. As can be seen in Figure 28a, a positive center vortex would produce a pattern that has a large, nearly round patch of aurora in the upper atmosphere with a dark, east-west-aligned feature within it. The dark feature corresponds to the magnetic footprint of the magnetospheric vortex, with the large region of aurora being predominantly outside the magnetic footprint. As can be seen in Figure 28b, a negative center vortex would produce a very different pattern, a pattern that has a narrow, east-west-aligned bright feature surrounded by darkness. The east-west-aligned bright feature corresponds to the magnetic footprint of the magnetospheric vortex.

As noted in Table 2, the total power dissipation is much larger (about 19 times as much) for the example positive center vortex than it is for the example negative center vortex. This being the case, the example positive center vortex will dissipate its kinetic energy 19 times faster than will the example negative center vortex. (This, of course, ignores the dynamics of the Alfven-wave coupling time to the ionosphere [e.g., *Goertz and Boswell*, 1979; *Goertz et al.*, 1993].) Hence one might expect to see more negative center vortices in the plasma sheet than positive center vortices.

7. Summary and Predictions

For flow vortices and flow channels in the magnetosphere magnetically connected to the resistive ionosphere, the dc electric-field pattern, the dc currents, and the amount of power dissipation were calculated. The calculations were a generalization to two dimensions in the ionosphere of earlier work that was one-dimensional. In section 7.1 the results of these calculations are summarized, and in section 7.2 a list of new predictions that are made from these results is generated.

7.1. Summary of Results

One of the basic findings is that negative charge imposed from the magnetosphere spreads across $\vec{B}$ as it connects along $\vec{B}$ to the ionosphere and, relatedly, upward field-aligned currents driven from the magnetosphere spread across $\vec{B}$ as they connect to the ionosphere. Positive charge imposed from the magnetosphere stays confined along $\vec{B}$ as it connects to the ionosphere and, relatedly, downward field-aligned currents driven from the magnetosphere remain confined along $\vec{B}$ as they connect to the ionosphere. The difference is due to the diode-like effect of field-aligned currents, where electron current carriers flowing into the dipole require a potential drop to overcome the mirror force whereas electron current carriers flowing out of the dipole do not [e.g., *Knight*, 1973].

A flow vortex in the magnetosphere has a radially converging or a radially diverging electric field that is confined between a central charge region and an outer

Figure 28. For (a) the example positive center vortex and (b) the example negative center vortex contained in Table 2, contour plots are shown of the logarithm of the power dissipation per unit area of the ionosphere P that is dissipated in upward field-aligned currents.

vortices: Figure 28a is for the positive center vortex, and Figure 28b is for the negative center vortex. The power dissipation in the upward currents is plotted because, as stated above, this power can lead to auroral airglow in the upper atmosphere owing to the acceleration of downgoing electrons. If the parameters of the example vortices had been chosen such that the magnetospheric velocities were larger or the magnetospheric magnetic field were larger, then the amount of parallel power dissipation would be sufficient to produce aurora

charge region (Figure 2). Owing to the difference in the geometries of the central-charge region and the outer-charge region, a positive center ($\vec{\Omega}$ antiparallel to $\vec{B}$) vortex and a negative center ($\vec{\Omega}$ parallel to $\vec{B}$) vortex will map differently to the ionosphere (see Table 1). Negative center vortices stay confined to their magnetic footprints and positive center vortices spread outside their magnetic footprints. Accounting for the shape of magnetospheric magnetic-field lines, circular vortices in the magnetosphere have magnetic footprints in the ionosphere that are east-west-aligned narrow structures (Figure 22). Negative center vortices, confined to the magnetic footprints, map down to east-west-aligned narrow vortices of flow in the ionosphere (Figure 25b). Positive center vortices, which spread outside their magnetic footprints, map down to quasi-circular vortices of flow in the ionosphere (Figure 25a). Owing to the coupling to the ionosphere, a positive center vortex will develop regions of back emf outside the vortex in the magnetosphere, producing a region of backspin outside the vortex in the magnetosphere. Negative center vortices do not develop this.

The smaller the magnetic footprint of a vortex, the poorer the penetration of its electric field down to the ionosphere (see Figures 4, 11, and 13). The penetration of the electric fields of negative center vortices down from the magnetosphere is weaker than is the penetration of the electric fields of positive center vortices (Figure 4). That is, negative center vortices couple poorly in comparison with positive center vortices (see Table 1).

Relatedly, negative center vortices have weaker current systems and dissipate less power than do positive center vortices (Figure 5 and see Table 1). For negative center vortices, if the magnetic footprint is not extremely large, most of the power they dissipate is dissipated in the upward-field-aligned current region, but if the footprint is extremely large, then most of the power they dissipate is in the Pedersen currents in the ionosphere (Figure 6). For positive center vortices, regardless of the size of their footprints, most of the power they dissipate is dissipated in the Pedersen currents in the ionosphere (Figure 6).

A strong enough vortex can produce enough power dissipation in the upward field-aligned currents to result in an aurora in the upper atmosphere owing to the energization of downgoing electrons. Looking at the patterns of aurora, it is predicted that a positive center vortex would produce a large circular region of aurora with a narrow east-west-aligned dark feature at its center (Figure 28a), somewhat like a black arc imbedded in diffuse glow. It is predicted that a negative center vortex would produce a narrow east-west-aligned bright feature (see Figure 28b), somewhat like an auroral arc.

Accounting for the fact that the magnetic footprint of a magnetospheric vortex is narrow and east-west aligned in the ionosphere, the question is asked, Which footprint scale size (east-west or north-south) is important

for determining the coupling of the vortex to the ionosphere? For positive center vortices, which spread outside the magnetic footprint, the answer is that the total amount of power dissipation is only weakly dependent on the footprint size (Figures 12 and 13b). For negative center vortices, which are confined to the magnetic footprint, the answer is that both scale sizes are equally important, with the total power dissipated being linearly proportional to the area of the footprint (Figures 12 and 11b).

Flow channels in the magnetotail (which will magnetically map to mostly east-west-aligned features in the ionosphere) have positive-charge edges and negative-charge edges (Figure 18). The positive-charge edges map along $\vec{B}$ to the ionosphere without spreading across $\vec{B}$, and the downward field-aligned currents at that edge map along $\vec{B}$ to the ionosphere without spreading (Figure 15). The negative-charge edges spread across $\vec{B}$ as they map along $\vec{B}$ to the ionosphere, and likewise the upward field-aligned current region connecting to the negative-charge edge broadens outside the magnetic footprint of the channel (Figure 15).

Associated with the spreading of the upward field-aligned current driven by the negative charge, a back emf will be produced in the magnetosphere outside the channel on the negative-charge edge (see Figure 18). This back emf will produce a backflow (opposite to the direction of the channel flow) outside the one edge of the channel in the magnetospheric plasma.

When the infinite-conductivity condition for the downward field-aligned-current regions is replaced with an Ohm's law with finite conductivity for flow vortices and flow channels in the magnetosphere, it is found that (1) the positive-charge regions and associated downward current regions are no longer confined to $\vec{B}$ as they map down $\vec{B}$ (Figures 19 and 20b), (2) negative center vortices are no longer confined to the magnetic footprint in the ionosphere (Figure 21b), (3) the coupling of positive center vortices to the ionosphere is greatly reduced as measured by the total power dissipation (Figure 21a), and (4) the coupling of negative center vortices to the ionosphere is not strongly affected.

7.2. New Predictions

Five predictions are made about vortices in the magnetosphere, about electric fields above the ionosphere, about auroral airglow signatures, and about flow channels in the magnetosphere. These predictions are (1) more $\vec{\Omega}$-parallel-to-$\vec{B}$ than $\vec{\Omega}$-antiparallel-to-$\vec{B}$ vortices in the magnetosphere, (2) more strong $\nabla_\perp \cdot E_\perp > 0$ than strong $\nabla_\perp \cdot E_\perp < 0$ above ionosphere, (3) $\vec{\Omega}$-antiparallel-to-$\vec{B}$ vortices produce east-west-aligned black aurora, (4) $\vec{\Omega}$-parallel-to-$\vec{B}$ vortices produce east-west-aligned arcs, and (5) plasma backflow adjacent to flow channels in magnetosphere.

The first prediction originates from the finding that positive center vortices dissipate much more power than

do negative center vortices (e.g., Figure 5, Figure 12, and Table 2). From this it is predicted that there should be more and stronger negative center vortices in the magnetosphere than positive center vortices. Recall that negative center vortices have $\vec{\Omega}$ parallel to $\vec{B}$ and when viewed from the $+z$ direction (looking down from the north) they have a counterclockwise rotation.

The second prediction originates from the finding that the electric fields of positive center vortices penetrate to the ionosphere much better than do the electric fields of negative center vortices (e.g., Figure 4, Figure 23, and Table 2). From this it is predicted that above the ionosphere on magnetic field lines that connect to regions where there are magnetospheric flow vortices (i.e., on field lines connecting to the magnetotail plasma sheet) there should be more regions of strong $\nabla_\perp \cdot \vec{E}_\perp > 0$ than there are regions of strong $\nabla_\perp \cdot \vec{E}_\perp < 0$. That is, if one should look at north-south satellite cuts through the nightside auroral zone and bin up the measured values of $\nabla_\perp \cdot \vec{E}_\perp$ (which is $\approx \nabla_{n\text{-}s} E_{n\text{-}s}$ where the subscript "n-s" stands for "north-south"), then one should find that the distribution has many more values of large positive $\nabla_{n\text{-}s} E_{n\text{-}s}$ than of large negative $\nabla_{n\text{-}s} E_{n\text{-}s}$.

The third prediction originates from the investigation of the pattern of power dissipation in the upward field-aligned currents driven by positive center vortices (e.g., Figure 28a). It is predicted that positive center vortices in the magnetosphere ($\vec{\Omega}$ antiparallel to $\vec{B}$) will produce patterns of aurora in the ionosphere that are large, circular patches of emission with a narrow east-west-aligned dark streak through them. The dark streak within the large aurora patch may be a black arc embedded in diffuse aurora [e.g., *Trondsen and Cogger*, 1997; *Kimball and Hallinan*, 1998]. In the vortex-coupling calculations, the dark regions are associated with $\nabla_\perp \cdot \vec{E}_\perp > 0$ (e.g., compare Figure 27a with Figure 23), as is the case for black aurora [e.g., *Marklund et al.*, 1994].

The fourth prediction originates from the investigation of the pattern of power dissipation in the upward field-aligned currents driven by negative center vortices (e.g., Figure 28b). It is predicted that a negative center vortex in the magnetosphere ($\vec{\Omega}$ parallel to $\vec{B}$) can produce a narrow east-west-aligned bright streak of aurora in the ionosphere. The bright streak may be an auroral arc. In the vortex-coupling calculations the narrow bright features are associated with $\nabla_\perp \cdot \vec{E}_\perp < 0$ (e.g., compare Figure 27b with Figure 23), as is the case for auroral arcs [e.g., *Hallinan*, 1981; *Lanchester et al.*, 1996].

The fifth prediction originates from the spreading across $\vec{B}$ of the upward field-aligned current that connects the ionosphere with the negative-charge side of a magnetospheric flow channel (e.g., Figure 18 and the bottom plot of Figure 15). After it spreads outside the magnetic footprint of the flow channel, this upward current will close in the magnetosphere outside of the channel by polarization-drift currents across $\vec{B}$, and this

closure will result in a $\vec{j} \times \vec{B}$ force on the magnetospheric plasma outside of the channel. The direction of the $\vec{j} \times \vec{B}$ force is such that it will produce a plasma flow in the direction opposite to the channel flow. This region of backflow will be produced off the negative-charge side of the channel. For a channel of flow in the magnetotail heading earthward, this backflow region will appear as a tailward flow off the dawnward side of the earthward-flowing channel.

References

Antonova, Y. Y., and V. A. Tverskoy, Nature of the electron precipitation band of the inverted V type and of the Harang discontinuity in the evening sector of the auroral ionosphere, *Geomagn. Aeron.*, *15*, 85, 1975.

Block, L. P., A double layer review, *Astrophys. Space Sci.*, *55*, 59, 1978.

Boehm, M. H., J. Clemmons, J.-E. Wahlund, A. Eriksson, L. Eliasson, L. Blomberg, P. Kintner, and H. Hofner, Observations of an upward-directed electron beam with the perpendicular temperature of the cold ionosphere, *Geophy. Res. Lett.*, *22*, 2103, 1995.

Borovsky, J. E., Limits on the cross-field propagation of streams of cold plasma, *Phys. Fluids, 30*, 2518, 1987.

Borovsky, J. E., Physics issues associated with low-β plasma generators, *IEEE Trans. Plasma Sci.*, *20*, 644, 1992.

Borovsky, J. E., Auroral arc thicknesses as predicted by various theories, *J. Geophys. Res.*, *98*, 6101, 1993.

Borovsky, J. E., and P. J. Hansen, The morphological evolution and internal convection of $\vec{E} \times \vec{B}$-drifting plasma clouds: Theory, dielectric-in-cell simulations, and N-body dielectric simulations, *Phys. Plasmas*, *5*, 3195, 1998.

Borovsky, J. E., R. C. Elphic, H. O. Funsten, and M. F. Thomsen, The Earth's plasma sheet as a laboratory for flow turbulence in high-β MHD, *J. Plasma Phys.*, *57*, 1, 1997.

Borovsky, J. E., M. F. Thomsen, R. C. Elphic, T. E. Cayton, and D. J. McComas, The transport of plasma-sheet material from the distant tail to geosynchronous orbit, *J. Geophys. Res.*, *103*, 20297, 1998.

Bostrom, R., Electrodynamics of the ionosphere, in *Cosmical Geophysics*, edited by A. Egeland, O. Holter, and A. Omholt, p. 181, Universitetsforlaget, Oslo, 1973.

Carlson, C. W., et al., FAST observations in the downward auroral current region: Energetic upgoing electron beams, parallel potential drops, and ion heating, *Geophys. Res. Lett.*, *25*, 2017, 1998.

Carpenter, R. T., and S. Torven, The current-voltage characteristics and potential oscillations of a double layer in a triple-plasma device, *IEEE Trans. Plasma Sci.*, *15*, 434, 1987.

Chen, F. F., Electric probes, in *Plasma Diagnostic Techniques*, edited by R. H. Huddlestone and S. L. Leonard, p. 113, Academic, San Diego, 1965.

Chiu, Y. T., and J. M. Cornwall, Electrostatic model of a quiet auroral arc, *J. Geophys. Res.*, *85*, 543, 1980.

Chiu, Y. T., A. L. Newman, and J. M. Cornwall, On the structures and mapping of auroral electrostatic potentials, *J. Geophys. Res.*, *86*, 10,029, 1981.

Collin, H. L., R. D. Sharp, and E. G. Shelley, The occurrence and characteristics of electron beams over the polar regions, *J. Geophys. Res.*, *87*, 7504, 1982.

Dalgarno, A., I. D. Latimer, and J. W. McConkey, Corpuscular bombardment and N_2^+ radiation, *Planet. Space Sci.*, *13*, 1008, 1965.

de la Beaujardiere, O., L. R. Lyons, J. M. Ruohoniemi, E. Friis-Christensen, C. Danielsen, F. J. Rich, and P. T. Newell, Quiet-time intensifications along the poleward auroral boundary near midnight, *J. Geophys. Res.*, *99*, 287, 1994.

Dors, E. E., and C. A. Kletzing, Effects of suprathermal tails on auroral electrodynamics, *J. Geophys. Res.*, *104*, 6783, 1999.

Elphic, et al., The auroral current circuit and field-aligned currents observed by FAST, *Geophys. Res. Lett.*, *25*, 2033, 1998.

Funsten, H. O., J. E. Borovsky, R. C. Elphic, and M. F. Thomsen, The turbulent flows of the plasma sheet, *Eos Trans. AGU, 76*(46), Fall Meet. Suppl., F486, 1995.

Galvez, M., Computer simulation of a plasma streaming across a magnetic field, *Phys. Fluids, 30*, 2729, 1987.

Goertz, C. K., Auroral arc formation: Kinetic and MHD effects, *Space Sci. Rev., 42*, 499, 1985.

Goertz, C. K., and R. W. Boswell, Magnetosphere-ionosphere coupling, *J. Geophys. Res., 84*, 7239, 1979.

Goertz, C. K., L.-H. Shan, and R. A. Smith, Prediction of geomagnetic activity, *J. Geophys. Res., 98*, 7673, 1993.

Haerendel, G., An Alfven wave model of auroral arcs, *High-Latitude Space Plasma Physics*, edited by B. Hultqvist and T. Hagfors, pp. 515-535, Plenum, New York, 1983.

Hallinan, T. J., The distribution of vorticity in auroral arcs, in *Physics of Auroral Arc Formation*, edited by S.-I. Akasofu and J. R. Kan, *Geophys. Monogr. Ser.*, vol. 25, p. 42, AGU, Washington, D.C., 1981.

Hultqvist, B., R. Lundin, K. Stasiewicz, L. Block, P.-A. Lindqvist, G. Gustafsson, H. Koskinen, A. Bahnsen, T. A. Potemra, and L. J. Zanetti, Simultaneous observation of upward moving field-aligned energetic electrons and ions on auroral zone field lines, *J. Geophys. Res., 93*, 9765, 1988.

Kaufmann, R. L., D. J. Larson, and C. Lu, Mapping and distortions of auroral structures in the quiet magnetosphere, *J. Geophys. Res., 95*, 7973, 1990.

Kimball, J., and T. J. Hallinan, A morphological study of black vortex streets, *J. Geophys. Res., 103*, 14,683, 1998.

Klumpar, D. M., Statistical distribution of the auroral electron albedo in the magnetosphere, in *Auroral Plasma Dynamics, Geophys. Monogr. Ser.*, vol. 80, edited by R. L. Lysak, p. 163, American Geophysical Union, Washington, 1993.

Klumpar, D. M., and W. J. Heikkila, Electrons in the ionospheric source cone: Evidence for runaway electrons as carriers of downward Birkeland currents, *Geophys. Res. Lett., 9*, 873, 1982.

Klumpar, D. M., J. M. Quinn, and E. G. Shelley, Counter-streaming electrons at the geomagnetic equator near 9 R_E, *Geophys. Res. Lett., 15*, 1295, 1988.

Knight, S., Parallel electric fields, *Planet. Space Sci., 21*, 741, 1973.

Lanchester, B. S., K. Kaila, and I. W. McCrea, Relationship between large horizontal electric fields and auroral arc elements, *J. Geophys. Res., 101*, 5075, 1996.

Lyons, L. R., Generation of large-scale regions of auroral currents, electric potentials, and precipitation by the divergence of the convection electric field, *J. Geophys. Res., 85*, 17, 1980.

Lyons, L. R., Discrete aurora as the direct result of an in-ferred high-altitude generating potential distribution, *J. Geophys. Res., 86*, 1, 1981.

Lysak, R. L., Electrodynamic coupling of the magnetosphere and ionosphere, *Space Sci. Rev., 52*, 33, 1990.

Marklund, G., L. Blomberg, C.-G. Falthammar, and P.-A. Lindqvist, On intense diverging electric fields associated with black aurora, *Geophys. Res. Lett., 21*, 1859, 1994.

McIlwain, C. E., Auroral electron beams near the magnetic equator, in *Physics of Hot Plasma in the Magnetosphere*, edited by B. Hultqvist and L. Stenfo, p. 91, Plenum, New York, 1975.

Meier, R. R., and D. J. Strickland, Auroral emission processes and remote sensing, in *Auroral Physics*, edited by C.-I. Meng, M. J. Rycroft, and L. A. Frank, p. 37, Cambridge Univ. Press, New York, 1991.

Montgomery, D., Remarks on the MHD problem of generic magnetospheres and magnetotails, in *Magnetotail Physics*, edited by A. T. Y. Lui, p. 203, Johns Hopkins Univ. Press, Baltimore, Md., 1987.

Newman, A. L., Y. T. Chiu, and J. M. Cornwall, Two-dimensional quasi-neutral description of particles and fields above discrete auroral arcs, *J. Geophys. Res., 91*, 3167, 1986.

Peredo, M., D. P. Stern, and N. A. Tsyganenko, Are existing magnetospheric models excessively stretched?, *J. Geophys. Res., 98*, 15,343, 1993.

Pudovkin, M. I., A. Steen, and U. Brandstrom, Vorticity in the magnetospheric plasma and its signature in the auroral dynamics, *Space Sci Rev., 80*, 411, 1997.

Roache, P. J., *Computational Fluid Dynamics*, sect. III-B-2, Hermosa, Albuquerque, N.M., 1976.

Robinson, R. M., E. A. Bering, R. R. Vondrak, H. R. Anderson, and P. A. Cloutier, Simultaneous rocket and radar measurements of currents in an auroral arc, *J. Geophys. Res., 86*, 7703, 1981.

Sandholt, P. E., Magnetopause plasma transients: Signatures in the auroral ionosphere, *J. Atmos. Terr. Phys., 55*, 1699, 1993.

Tennekes, H., and J. L. Lumley, *A First Course in Turbulence*, sect. 3.3, MIT Press, Cambridge, Mass., 1972.

Tritton, D. J., *Physical Fluid Dynamics*, sect. 6.4, Van Nostrand Reinhold, New York, 1977.

Trondsen, T. S., and L. L. Cogger, High-resolution television observations of black aurora, *J. Geophys. Res., 102*, 363, 1997.

Tsyganenko, N. A., A magnetospheric magnetic field model with a warped tail current sheet, *Planet. Space Sci., 37*, 5, 1989.

Tsyganenko, N. A., Effects of the solar wind conditions on the global magnetospheric configuration as deduced from data-based field models, in *Proceedings of the Third International Conference on Substorms, Eur. Space Agency Spec. Publ., ESA SP-389*, 181, 1996.

Weimer, D. R., C. K. Goertz, D. A. Gurnett, N. C. Maynard, and J. L. Burch, Auroral zone electric fields from DE 1 and 2 at magnetic conjunctions, *J. Geophys. Res., 90*, 7479, 1985.

Zhang, D. Y., and K. D. Cole, Some aspects of electric field mapping in the auroral ionosphere, *Planet. Space Sci., 35*, 1513, 1987.

J. Bonnell, Space Sciences Lab, University of California, Berkeley, CA 94720-7450. (email: jbonnell@ssl.berkeley.edu)

J. E. Borovsky, Space and Atmospheric Sciences, Mail Stop D466, Los Alamos National Laboratory, Los Alamos, NM 87545. (email: jborovsky@lanl.gov)